THE ASTROPHYSICAL JOURNAL, 340:273–297, 1989 May 1

INTERSTELLAR C_2, CH, AND CN IN TRANSLUCENT MOLECULAR CLOUDS[1,2]

EWINE F. VAN DISHOECK[3,4]
Harvard-Smithsonian Center for Astrophysics and Princeton University Observatory
AND
JOHN H. BLACK[3]
Steward Observatory
Received 1988 June 27; accepted 1988 October 3

ABSTRACT

Optical absorption-line techniques have been applied to the study of a number of translucent molecular clouds in which the total column densities are large enough that substantial molecular abundances can be maintained. Results are presented for a survey of absorption lines of interstellar C_2, CH, and CN. Detections of CN through the $A\ ^2\Pi$–$X\ ^2\Sigma^+$ (1, 0) and (2, 0) bands of the red system are reported, and are compared with observations of the violet system for one line of sight. The population distributions in C_2 provide diagnostic information on temperature and density. The measured column densities of the three species can be used to test details of the theory of molecule formation in clouds where photoprocesses still play a significant role. The C_2 and CH column densities are strongly correlated with each other and probably also with the H_2 column density. In contrast, the CN column densities are found to vary greatly from cloud to cloud. The observations are discussed with reference to detailed theoretical models.

Subject headings: interstellar: abundances — interstellar: molecules — molecular processes

I. INTRODUCTION

The study of interstellar clouds has traditionally been concerned with two different classes of clouds. Diffuse clouds, which have a total visual extinction $A_V^{tot} \leq 2$ mag, have been observed through absorption lines of atoms and molecules at visible and ultraviolet wavelengths in the spectra of background stars. Photoprocesses, such as photodissociation and photoionization of the molecules and atoms, play an important role in the physical and chemical structure of these clouds, and the fractional ionization is consequently high [$n(e)/n_H \approx 10^{-4}$]. Dense and dark molecular clouds, which typically have $A_V^{tot} > 10$ mag and much larger molecular column densities, have been studied by emission lines of molecules at centimeter and millimeter wavelengths. Owing to the large extinction, photoprocesses are generally thought to be negligible inside molecular clouds, and the inferred electron abundances are much lower. Few studies exist of clouds with $A_V^{tot} \approx 2$–10 mag [$E(B-V) \approx 0.7$–3], which occupy the middle ground of parameter space between the diffuse and dense molecular clouds (Crutcher 1985). With the advent of more efficient detectors, these clouds are now amenable to study not only by radio techniques but also through optical absorption-line observations. We will denote those clouds with $A_V^{tot} \gtrsim 2$ mag, which show strong molecular absorption lines, as "translucent molecular clouds." Note that this is a strictly empirical distinction based primarily on cloud thickness and molecular column densities. Although the translucent clouds are usually taken to refer to isolated small clouds, they may also represent the outer edges of dense molecular clouds. It is the aim of this paper to investigate the chemical state of translucent clouds in more detail through absorption-line observations combined with detailed theoretical models.

The relative merits of each of the two observational techniques for the study of the physical and chemical structure of interstellar clouds have been discussed by Crutcher (1985). In short, the main advantages of the radio measurements are (1) their routinely high spectral resolution ($\lambda/\Delta\lambda \approx 10^6$–$10^7$, or 0.03–0.3 km s^{-1} in Doppler velocity), so that the line profiles are resolved; (2) the fact that most lines are seen in emission, so that it is possible to map the spatial distribution of the clouds; and (3) the fact that complex molecules are more readily detected at millimeter than at optical wavelengths, so that the radio results may provide more information on interstellar chemistry. On the other hand, the optical technique has the advantages that (1) a background star yields an angular resolution about 10^5 times higher than that of radio emission-line methods and ensures that the same absorbing column of the cloud is sampled in all measurements; (2) the derivation of column densities is more reliable and straightforward than for radio data; (3) important molecules, such as H_2 and C_2, can be observed at visible and ultraviolet wavelengths, but not at radio wavelengths; (4) lines of atoms in various stages of ionization can be measured, so that direct information on the depletion of the elements in the cloud can be obtained as well as an estimate of the electron abundance; and finally (5) the extinction and polarization can be measured for the same absorbing column, so that information on the properties of the dust in the cloud can be obtained.

The main drawback of the optical absorption-line observations is the requirement of a suitable background star. Relatively few bright stars behind molecular clouds have been identified. Münch (1964) reported very strong lines of CN in the spectrum of the heavily reddened star BD +66°1675.

[1] Based on observations collected at the European Southern Observatory, La Silla, Chile.
[2] Based on observations made with the Multiple Mirror Telescope, a joint facility of the University of Arizona and the Smithsonian Institution.
[3] Visiting Astronomer, Cerro Tololo Inter-American Observatory, National Optical Astronomy Observatories, operated by the Association of Universities for Research in Astronomy, Inc., under contract with the National Science Foundation.
[4] Junior Fellow, Harvard Society of Fellows.

Cohen (1973) searched for atomic and molecular lines at blue wavelengths in photographic spectra of relatively low resolution toward about 30 stars with large extinctions. Strong molecular lines were found for only a few lines of sight, although marginal detections were reported toward about half the stars. In subsequent years, additional translucent clouds have been found through searches either for the absorption lines of the CH, CH^+, or CN molecules at blue wavelengths (Blades and Bennewith 1973; Dickman *et al.* 1983; Crutcher 1985; Crutcher and Chu 1985; Cardelli and Wallerstein 1986) or for lines of the C_2 molecule at red wavelengths (Souza and Lutz 1977; Hobbs, Black, and van Dishoeck 1983; Lutz and Crutcher 1983; van Dishoeck and de Zeeuw 1984; Gredel and Münch 1986; Jannuzi *et al.* 1988; Federman and Lambert 1988). Millimeter emission-line studies are lacking for most of these clouds. Dickman *et al.* (1983) reported the detection of the CO $J = 1 \rightarrow 0$ emission line for a few lines of sight. More recently, Lada and Blitz (1988) have studied the CO emission from a sample of diffuse and translucent clouds, and Jannuzi *et al.* (1988) have mapped the small molecular cloud in front of HD 169454 in CO. The most comprehensive study to date of a translucent cloud through combined optical and millimeter measurements is that of Crutcher (1985) toward HD 29647. This heavily reddened late B star lies in or behind a substantial part of the darkest portion of the Taurus molecular cloud complex.

Because of the still limited number of background stars, we decided to perform a search for interstellar molecular absorption lines toward highly reddened stars in the southern sky. Preliminary results of the observations were reported in van Dishoeck and Black (1984, 1985, 1986*b*). The second goal of this study is to test theories of interstellar chemistry by comparing the observations of simple molecules with predictions from comprehensive models over a larger range of cloud thickness than was possible previously (van Dishoeck and Black 1986*a*, 1988*a*). Details of the observations and the method of analysis are presented in § II. Results of the observations for individual lines of sight are presented in § III, and general relations between the various species are discussed in § IV. Finally, the observations are compared with model results in § V.

II. METHOD

a) Spectroscopic Considerations

Because of the reduced extinction at longer wavelengths, we searched primarily for the C_2 $A\ ^1\Pi_u$–$X\ ^1\Sigma_g^+$ Phillips system at 8750 Å. Observations of the homonuclear C_2 molecule have the additional advantage that the measured rotational population distribution provides information on the physical conditions in the clouds, such as temperatures and densities (van Dishoeck and Black 1982). For those lines of sight for which C_2 was detected, we also searched for CN and CH. Although interstellar CN is commonly observed in diffuse clouds by its strong absorption lines in the $B\ ^2\Sigma^+$–$X\ ^2\Sigma^+$ (0, 0) violet system at 3875 Å, we decided to focus on the weaker lines in the $A\ ^2\Pi$–$X\ ^2\Sigma^+$ (2, 0) and (1, 0) red bands. For highly reddened lines of sight, the reduced extinction at 7900 Å easily compensates for the order-of-magnitude smaller oscillator strength. An additional advantage of the red system compared with the violet system is that the lines are even less likely to be saturated because of their smaller strength. The only major disadvantage is the fact that both the A–X (2, 0) band at 7900 Å and the (1, 0) band at 9135 Å lie in wavelength regions where numerous atmospheric features occur. Lines of the CN red system have long been observed in the spectra of stellar (Miller 1953; McKellar 1954) and cometary (Dufay and Swings 1958) atmospheres, but none had been reported in interstellar clouds prior to this work. For CH, we observed the longest wavelength $A\ ^2\Delta$–$X\ ^2\Pi$ system at 4300 Å.

b) Selection of Stars

The suitability of a star for observations of lines of interstellar C_2 around 8750 Å depends upon (1) the amount of foreground interstellar matter; (2) the apparent brightness of the star at 8750 Å; (3) the sensitivity of the telescope, spectrograph, and detector; and (4) the absence of confusing stellar absorption lines. Only early-type stars with reddening $E(B-V) > 0.5$ were considered. Apparent magnitudes in the I band ($\lambda_{\rm eff} \approx 9000$ Å), $I \lesssim 8$ mag, are required for observations at the highest resolution; when the reddening is large, the corresponding visual magnitude may be $V \approx 10$ mag. The initial list of stars was based on the catalogs of Garrison, Hiltner, and Schild (1977), Klare and Neckel (1977), and Humphreys (1978). Further sources of data on photometry and spectral types of the stars were Schild, Garrison, and Hiltner (1983), Conti *et al.* (1983), Leitherer and Wolf (1984), Whittet and van Breda (1980), and Castor and Simon (1983). A few individual stars were added to the list based on their specific interest. Priority was given to those stars which lie close to, or possibly behind, known southern dark cloud complexes, such as the Coalsack, the Ophiuchus and Chamaeleon dark cloud regions, and the Carina OB1 association. The final list of stars observed is presented in Table 1. Note that many of the stars in the list are distant supergiants, for which it was not known *a priori* whether the large reddening arises from a long path length through an average thin interstellar medium or whether the line of sight passes through a dense cloud.

c) Observations and Reduction

Observations of interstellar absorption lines of C_2 in the Phillips $A\ ^1\Pi_u$–$X\ ^1\Sigma_g^+$ (2, 0) band system around 8750 Å were performed at the 1.4 m coudé auxiliary telescope (CAT) of the European Southern Observatory (ESO) and at the 4 m telescope of the Cerro Tololo Inter-American Observatory (CTIO). At ESO, observations were made in the periods 1984 August 21–28 and 1985 March 18–24 with the coudé echelle spectrograph (CES), which was equipped with an unintensified Reticon detector consisting of a linear array of 1872 photodiodes cooled to 140 K (Enard 1981). The resolving power was set to $R = \lambda/\Delta\lambda = 80{,}000$ or $\Delta\lambda = 109.8$ mÅ at $\lambda = 8781$ Å, corresponding to a reciprocal dispersion of 2.45 Å mm^{-1} or a velocity resolution of 3.8 km s^{-1}. The entrance slit was projected onto 3 diodes of the array. The detector was centered at 8781 Å, so that the resulting spectra covered the 8745–8812 Å range. This wavelength region includes all P, Q, and R lines of the C_2 (2, 0) Phillips band of practical interest. Wavelength calibration was established by emission lines from a Th-Ar hollow cathode lamp. Accurate thorium wavelengths were taken from Palmer and Engelman (1983). These calibration measurements allow a determination of the absolute wavelength scale to better than 3 mÅ. The initial exposure time for each line of sight was 1–1½ hours. For those stars whose initial spectra showed clear absorption lines of interstellar C_2, additional exposures were obtained up to total exposure times of 5–6 hr. Flat-field spectra were taken immediately before and

TABLE 1

PROPERTIES OF THE OBSERVED STARS

Star	l	b	Sp. type	V	I	$E(B-V)$	Distance (pc)	Remarks
JM-1	206.528	-16.378	B0.5Vp	12.2	8.7	1.69	450	NGC 2024 IRS1
HDE 290861	205.176	-14.128	B3	10.1	8.2	1.25	500	NGC 2071
HD 63804	248.767	-3.710	B9.5Ia$^+$e	7.8	5.6	1.19	3200	near NGC 2439
HD 75149	265.332	-1.692	B3Ia	5.5	4.9	0.41	1800	Vel OB1
HD 78344	268.888	-0.375	O9.5Ia	9.0	7.2	1.40	1700	
HD 80077	271.629	-0.674	B2Ia$^+$e	7.6	5.2	1.52	3000	Pişmiş 11
HD 80558	273.074	-1.466	B6Ia	5.8	4.7	0.62	1500	
HD 92693	286.293	+0.655	A2Ia	7.0	5.0	1.02	2500	Car OB1,
HD 94413	296.256	-15.842	B2V	8.0	7.3	0.81	400	Cha dark cloud
HD 94910	289.183	-0.695	B2 pe	7.0	5.7:	0.55:	2000	AG Car
HD 97300	297.033	-14.919	B9V	9.1	8.3	0.44	160	Cha dark cloud
HD 106391	298.600	+0.659	B2.5Ia	8.6	7.1	0.92	3500	Coalsack
Wray 977	300.097	-0.035	B2Iae	10.8	7.6	1.9	2300	4U1223-62
HD 110432	301.958	-0.203	B1 pe	5.4	4.7	0.52	430	Coalsack
HD 112272	303.487	-1.494	B0.5Ia	7.3	5.8	1.05	2500	Coalsack, Cen OB1
HD 113422	304.493	+1.122	B1Iabp	8.2	6.9	1.02	2500	Coalsack, Cen OB1
HD 115842	307.081	+6.834	B0.5Iab	6.0	5.5	0.52	1300	
HD 134959	320.514	-1.208	B2Ia$^+$	8.1	6.2	1.20	4000	Pişmiş 20
CPD-57°7059	322.464	-1.334	B9Ib	9.7	7.0	1.43	700	
HD 147084	352.328	+18.050	A5II	4.6	3.0	0.74	170	o Sco
HD 147889	352.857	+17.044	B2V	7.9	6.2	1.09	170	In ρ Oph cloud
Elias 16	352.894	+16.847	B5:	12.0	9.1	2.1	170	In ρ Oph cloud
HD 148379	337.246	+1.576	B1.5Ia	5.4	4.4	0.69	1400	Ara OB1a
HD 152235	343.311	+1.104	B1I	6.3	5.4	0.77	1900	Sco OB1
HD 152236	343.028	+0.870	B1Iae	4.8	3.9	0.66	1900	Sco OB1
HD 154368	349.970	+3.215	O9.5Iab	6.1	5.4	0.82	800	
HD 156738	351.178	+0.483	O6.5III(f)	9.4	7.8	1.18	1900	NGC 6334
HD 157038	349.955	-0.794	B3Iap	6.3	5.1	0.89	1000	
HD 160529	355.702	-1.732	A2Iae	6.7	4.5	1.23	700	V905 Sco
HD 166734	18.920	+3.628	O7.5If	8.4	6.6	1.41	1400	
HD 168607	14.968	-0.940	B9Ia$^+$p	8.3	5.4	1.60	2200	Ser OB1
BD-14°5037	16.928	-0.951	B1.5Ia$^+$	8.2	5.8	1.57	1700	Sct OB3
HD 169454	17.539	-0.670	B1.5Ia	6.6	4.8	1.14	1700	V430 Sct, Sct OB3
HD 169754	20.023	+0.239	B0.5Ia	8.4	6.7	1.31	1800	
HD 181615	21.839	-13.774	B2Vpe+A2Ia	4.6	4.2	?	?	υ Sgr
HDE 229059	75.699	+0.401	B2Iabe	8.7	5.8	1.70	1800	Cyg OB1, ON2 region
BD +66°1675	118.214	+4.990	O7	9.1	7.0	1.4	840	NGC 7822, Cep OB4
Stars with previously published observations								
HD 23180	160.363	-17.740	B1III	3.8	3.7	0.30	330	o Per
HD 24398	162.289	-16.690	B1Ib	2.9	2.6	0.32	330	ζ Per
HD 29647	174.053	-13.349	B7III-IVp	8.3	6.8	1.04	140	Near TMC 1
HD 147933	353.687	+17.688	B2IV	5.0	4.2	0.41	170	ρ Oph
HD 148184	357.933	+20.677	B2IV:pe	4.4	3.7	~0.4	170	χ Oph
HD 149404	340.538	+3.006	O9Iae	5.5	4.7	0.74	1400	Ara OB1a
HD 149757	6.281	+23.588	O9.5Vn	2.6	2.5	0.33	170	ζ Oph
Cyg OB2 No. 12	80.102	+0.830	B8Ia^{++}	11.5	5.6	3.27	1800	Cyg OB2

NOTE.—Where applicable, stellar distances are based upon mean distances of clusters and associations (e.g., Humphreys 1978); otherwise, spectroscopic parallaxes based upon absolute magnitudes of Conti *et al.* 1983, Balona and Crampton 1974, and Walborn 1972 are used.

after each exposure and were used to correct the stellar exposures for pixel-to-pixel sensitivity variations. In addition, each stellar and flat-field exposure was corrected for the readout noise of the detector. Searches for lines of the interstellar CN $A\ ^2\Pi$–$X\ ^2\Sigma^+$ (2, 0) red system at 7900 Å were made with the CES at the same resolving power. Lines of interstellar CH in the $A\ ^2\Delta$–$X\ ^2\Pi$ (0, 0) band were observed with the CES by centering the detector at 4300 Å. All spectra were reduced using the ESO IHAP software package (Middleburg 1981). Note that even in the high-resolution spectra obtained at ESO, the interstellar lines are not resolved. Their widths are generally in harmony with a value of the Doppler parameter $b \lesssim 2$ km s^{-1}. The small aperture of the telescope and the sensitivity of the detector limited the C_2 observations at ESO to stars with an I-magnitude brighter than 6. Additional spectra of interstellar CH were obtained at the ESO CAT equipped with the new CCD detector at a resolving power $R \approx 70{,}000$ in 1987 July and December.

Observations of interstellar C_2 in the spectra of fainter stars with $I \leq 8$ mag were made at the CTIO 4 m telescope on 1985 April 1 and 2 using the echelle spectrograph with the long camera and a CCD detector. The resolving power of these measurements was $R \approx 36{,}000$, corresponding to a reciprocal dispersion of 4.86 Å mm^{-1} or a velocity resolution of 8.4 km s^{-1}. The detector was a GEC CCD with 576 × 385 pixels and a pixel size of 22 μm square. Owing to the small format of the detector and the optical design of the spectrograph, only portions of two orders of the spectrum could be observed at once. By good fortune, it was possible to obtain a single setting that centered on the principal interstellar lines of the C_2 $A\ ^1\Pi_u$–$X\ ^1\Sigma_g^+$ (2, 0) and CN $A\ ^2\Pi$–$X\ ^2\Sigma^+$ (1, 0) bands in the adjacent orders, at wavelengths 8768 and 9134 Å, respectively. The wavelength coverage was 8738–8800 Å and 9102–9166 Å, which unfortunately excluded the strongest CN line, (1, 0) $R_1(0)$ at 9186.935 Å. Typical exposure times were 20 minutes. At least two exposures were taken of those stars which clearly

showed interstellar C_2 lines in the spectrum after the first exposure. The images were corrected for bias and flat-fielding, and the wavelength scale was established by taking exposures of a Th-Ar comparison lamp before and after each set of stellar exposures. This procedure yields a wavelength scale accurate to 0.06 Å. In the 9135–9150 Å region, where few thorium lines are available for calibration, the positions of numerous telluric H_2O lines in the source spectra themselves allow a more accurate (to ± 0.02 Å) wavelength calibration. The data reduction was carried out using the NOAO/KPNO IRAF system. The reduction procedure consisted of an order-locating step, an extraction step in which the integrated one-dimensional spectrum is determined, and a measurement step. As will be discussed in § III*a*, a critical test of the reliability of the results has been performed by comparing observations of interstellar C_2 obtained both at ESO and at CTIO for the same line of sight.

Additional observations of interstellar CH were performed with the Multiple Mirror Telescope (MMT) and echelle spectrograph in 1985 October 27–29 and 1986 May 23–25, in order to reach stars that are too faint in the blue for observations of higher resolution at ESO. The one-dimensional intensified Reticon detector provided coverage of 43 Å centered on 4300 Å at a resolving power of $R = 24{,}000$, corresponding to a velocity resolution of 12.5 km s^{-1}. Typical exposures were 20 minutes, and two or more exposures were made on each star. Wavelengths were determined with reference to a Th-Ar comparison spectrum that was recorded after each stellar exposure.

d) Oscillator Strengths

Column densities for unsaturated lines were derived from the measured equivalent widths W_λ (in Å) under the assumption of a linear relationship

$$N_l = 1.13 \times 10^{20} \frac{W_\lambda^{ul}}{f_{ul}\lambda_{ul}^2} \text{ cm}^{-2}, \quad (1)$$

where N_l is the column density of the molecule in the lower level of the transition involved, λ_{ul} is the transition wavelength (in Å), and f_{ul} is the line absorption oscillator strength.

Line oscillator strengths $f_{J'J''}$ between rotational level J' of the upper state and J'' of the lower state were obtained from the band oscillator strength $f_{v'v''}$ between vibrational levels v' and v'' according to

$$f_{J'J''} = f_{v'v''}\left[\frac{\nu_{J'J''}}{\nu_{\text{band}}}\frac{\mathcal{S}_{J'J''}}{(2J''+1)}\right] \equiv f_{v'v''}\, p_{J'J''}, \quad (2)$$

where $\nu_{J'J''}$ and ν_{band} are the wavenumbers of the line and the band center, respectively. The $\mathcal{S}_{J'J''}$ are the Hönl-London rotational line intensity factors normalized such that $\sum_{J'} \mathcal{S}_{J'J''}/g_e(2J''+1) = 1$, and g_e is the ratio of electronic degeneracy factors ($g_e = 2$ for the A–X systems of C_2 and CN, and $g_e = 1$ for the A–X system of CH). The term in square brackets is denoted by $p_{J'J''}$. Transition wavelengths and values of $p_{J'J''}$ for various species are collected in Table 2. Note that for CH, only lines out of the lowest rotational level of the

TABLE 2

ADOPTED MOLECULAR DATA

Species	Transition	Line	J''	N''	λ^a	f_{band}	$p_{J'J''}$
C_2	$A\ ^1\Pi_u$–$X\ ^1\Sigma_g^+$ (2, 0)	$R(0)$	0	...	8757.6817	1.0(−3)	1.00
		$R(2)$	2	...	8753.9458		0.400
		$Q(2)$	2	...	8761.1898		0.500
		$Q(4)$	4	...	8763.7401		0.500
		$Q(6)$	6	...	8767.7504		0.500
CN	$A\ ^2\Pi$–$X\ ^2\Sigma^+$ (1,0)	$R_1(0)$	1/2	0	9186.935	1.5(−3)	0.528
		$^RQ_{21}(0)$	1/2	0	9144.043		0.334
		$^SR_{21}(0)$	1/2	0	9139.677		0.138
		$^QR_{12}(1)$	1/2	1	9190.110		0.468
		$Q_2(1)$	1/2	1	9147.201		0.334
		$R_2(1)$	1/2	1	9142.833		0.198
		$Q_1(1)$	3/2	1	9190.120		0.223
		$R_1(1)$	3/2	1	9183.216		0.334
		$^QP_{21}(1)$	3/2	1	9147.210		0.084
		$^RQ_{21}(1)$	3/2	1	9142.842		0.243
		$^SR_{21}(1)$	3/2	1	9135.571		0.116
	$A\ ^2\Pi$–$X\ ^2\Sigma^+$ (2, 0)	$R_1(0)$	1/2	0	7906.601	7.6(−4)	0.528
		$^RQ_{21}(0)$	1/2	0	7874.847		0.334
		$^SR_{21}(0)$	1/2	0	7871.643		0.138
		$^QR_{12}(1)$	1/2	1	7908.952		0.469
		$Q_2(1)$	1/2	1	7877.189		0.334
		$R_2(1)$	1/2	1	7873.983		0.198
		$Q_1(1)$	3/2	1	7908.959		0.224
		$R_1(1)$	3/2	1	7903.896		0.334
		$^QP_{21}(1)$	3/2	1	7877.196		0.084
		$^RQ_{21}(1)$	3/2	1	7873.990		0.244
		$^SR_{21}(1)$	3/2	1	7868.653		0.116
CH	$A\ ^2\Delta$–$X\ ^2\Pi$ (0, 0)	$R_2(1)^b$	1/2	...	4300.3132	5.06(−3)	1.0

[a] Rest wavelength in air in Å.

[b] This is an unresolved Λ-doublet; see text.

ground state can be observed. For the heavier CN molecule, the rotational levels lie sufficiently close in energy that the lowest few excited rotational levels are also populated significantly under interstellar conditions. The population of the homonuclear C_2 molecule is distributed over many rotational levels in interstellar clouds. Only lines out of the lowest few levels are listed in Table 2. More information can be found in van Dishoeck and de Zeeuw (1984). Very recently, improved line positions in the Phillips system have become available (Douay, Nietmann, and Bernath 1988).

The band oscillator strength of the CH $A\ ^2\Delta$–$X\ ^2\Pi$ (0, 0) transition is well determined, $f_{00} = 5.06 \times 10^{-3}$ (Larsson and Siegbahn 1983; Brzozowski *et al.* 1976). The oscillator strengths for the red systems of C_2 and CN remain controversial. The various recent experiments for the C_2 A–X Phillips system are consistent with $f_{00} \approx 1.8 \times 10^{-3}$ (Erman *et al.* 1982; Bauer *et al.* 1985, 1986; Davis *et al.* 1984), which implies $f_{20} \approx 1.0 \times 10^{-3}$. These measurements are about a factor of 2 lower than the early theoretical calculations which gave $f_{00} \approx 2.7 \times 10^{-3}$ (van Dishoeck 1983; Chabalowki, Peyerimhoff and Buenker 1983; Pouilly *et al.* 1983). Recent more extensive calculations by ONeil, Rosmus, and Werner (1987) and Klotz (1987) give somewhat lower values, $f_{00} \approx (2.2\text{–}2.3) \times 10^{-3}$. The remaining discrepancy between theory and experiment is not yet understood. In view of the good agreement among the latest experimental determinations, we have adopted $f_{20} = 1.0 \times 10^{-3}$ for the C_2 A–X (2, 0) band system. Note that this oscillator strength is smaller than $f_{20} = 1.7 \times 10^{-3}$ adopted in the analyses of previous observations (van Dishoeck and de Zeeuw 1984; van Dishoeck 1984; Hobbs, Black, and van Dishoeck 1983; van Dishoeck and Black 1986*a*), so that all column densities derived in that work need to be scaled upward by a factor of 1.7.

A similar discrepancy between theory and experiments exists for the $A\ ^2\Pi$–$X\ ^2\Sigma^+$ red system of CN. Various theoretical calculations for the (2, 0) band give $f_{20} = (1.25\text{–}1.7) \times 10^{-3}$ (Cartwright and Hay 1982; Larsson, Siegbahn, and Ågren 1983). The most recent experimental determination is $f_{20} = 7.6 \times 10^{-4}$ (Davis *et al.* 1986), a value which agrees well with other experimental results (Taherian and Slanger 1984) and the oscillator strength determined from an analysis of the solar spectrum (Sneden and Lambert 1982). Results of very recent, very elaborate quantum chemical calculations give $f_{20} = 9.1 \times 10^{-4}$ (Bauschlicher, Langhoff, and Taylor 1988). We have adopted the experimental oscillator strengths $f_{20} = 7.6 \times 10^{-4}$ and $f_{10} = 1.5 \times 10^{-3}$ in the analyses. Note that the oscillator strength of the CN $B\ ^2\Sigma^+$–$X\ ^2\Sigma^+$ (0, 0) band is well established to be $f_{00} = (3.2 \pm 0.2) \times 10^{-2}$ (Larsson, Siegbahn, and Ågren 1983; Davis *et al.* 1986). One interstellar region in which both violet and red system lines of CN are observed is discussed below (§ III*f*).

The oscillator strengths for the observed C_2 and CN transitions are weak enough that the lines are usually optically thin. However, the strongest lines of CH are slightly saturated. In those cases, column densities were obtained from curves of growth with $b = 1.0$ km s^{-1}, unless specified otherwise. Note that the CH feature at 4300 Å is actually a blend of two closely spaced lines (Λ-components) that arise in the two Λ-doubling sublevels of the ground state. The mean wavelength of the blend is 4300.3132 Å (in air), and the separation of the components is 0.0205 Å or 1.43 km s^{-1}, based upon the spectroscopic data of Brazier and Brown (1984) and Bernath (1987) as discussed by Black and van Dishoeck (1988). Table 3 compares the curve of growth that is obtained if the CH feature is assumed to consist of a single line with that in the more realistic case of a blend of two equally strong lines with equal population in the two Λ-doublet levels. It is apparent that for Doppler line-broadening parameters $b \approx 1$ km s^{-1}, the two approaches start to differ significantly for $W_\lambda \geq 20$ mÅ. The saturation corrections in this work are at most a factor of 2 in column density for the strongest CH lines observed.

e) C_2 *Rotational Excitation*

As discussed by van Dishoeck and Black (1982), the observed C_2 rotational population distribution provides information on the temperature and density in the cloud. The C_2 rotational level populations are determined by the competition between radiative pumping and collisional processes in the cloud. The resulting nonthermal rotational distributions can be characterized by the kinetic temperature T in the cloud and the combination of parameters $n\sigma_0/I_R$, where $n = n(\mathrm{H}) + n(\mathrm{H_2})$ is the density of collision partners in the cloud, I_R is

TABLE 3

CH CURVE OF GROWTH

	b[b] = 1.5		b = 1.0		b = 0.8		b = 0.7		b = 0.5	
N[a]	Blend[c]	Single[d]	Blend	Single	Blend	Single	Blend	Single	Blend	Single
5.0(12).....	4.0	4.0	4.0	3.9	4.0	3.9	4.0	3.8	3.9	3.7
1.0(13).....	7.8	7.7	7.7	7.4	7.6	7.2	7.6	7.1	7.4	6.7
2.0(13).....	14.7	14.3	14.3	13.3	14.0	12.7	13.9	12.3	13.3	11.0
3.0(13).....	20.8	20.0	19.9	18.1	19.5	16.9	19.2	16.1	18.0	14.0
4.0(13).....	26.2	25.0	24.8	22.1	24.1	20.2	23.6	19.1	21.9	16.1
5.0(13).....	31.0	29.3	29.0	25.3	28.0	22.9	27.3	21.4	25.0	17.6
7.0(13).....	39.2	36.4	35.8	30.2	34.2	26.7	33.1	24.7	29.7	19.7
1.0(14).....	48.6	44.3	43.2	35.2	40.6	30.5	39.1	27.8	34.3	21.7
2.0(14).....	66.1	58.3	55.5	43.4	50.6	36.5	47.9	32.8	41.1	25.0
3.0(14).....	74.6	65.1	60.8	47.3	54.6	39.5	51.3	35.3	43.8	26.6
5.0(14).....	83.4	72.4	66.2	51.8	58.7	42.9	54.7	38.2	46.3	28.6
1.0(15).....	93.2	81.1	72.3	57.2	63.4	47.0	58.7	41.8	49.1	31.1

[a] Total CH column density in cm^{-2}.
[b] Doppler parameter in km s^{-1}.
[c] Equivalent width in mÅ for blend of two CH lines; see text for details.
[d] Equivalent width in mÅ for the conventional—but incorrect—single CH line.

the scaling factor for the radiation field in the far-red part of the spectrum, and σ_0 is the cross section for collisional deexcitation. The inferred temperature is constrained mainly by the populations of the lowest few rotational levels. The inferred density n is uncertain by a factor of at least 2 for several reasons. First, the rotational level populations calculated by van Dishoeck and Black (1982; see also van Dishoeck 1984) used the theoretical oscillator strengths of van Dishoeck (1983) for the radiative pumping through the Phillips $A\ ^1\Pi_u$–$X\ ^1\Sigma_g^+$ system. These oscillator strengths are a factor of 1.7 larger than the value adopted in this work for the conversion of measured equivalent widths to column densities. The simplest way to incorporate the smaller oscillator strengths into the theory is to rescale the strength of the far-red radiation field (cf. van Dishoeck and Black 1982) accordingly. This results in an intensity of $8 \times 10^5\ I_R$ photons s^{-1} cm^{-2} $Å^{-1}$ at the relevant wavelength for excitation of 10000 Å, which is close for $I_R = 1$ to the intensity of 6×10^5 photons s^{-1} cm^{-2} $Å^{-1}$ at 10000 Å estimated by Mathis, Mezger, and Panagia (1983) for the Galactic background in the solar neighborhood. Note that with this rescaling procedure, the previously inferred densities of van Dishoeck and de Zeeuw (1984) and van Dishoeck (1984) are not affected. Second, the collisional cross section σ_0 is still uncertain by at least a factor of 2. In addition, the dependence of the cross section on rotational quantum number J has not been considered in the theory, although the J-dependent statistical weight factors that relate upward and downward rate coefficients are included. The value of σ_0 has been calibrated approximately to be $\sigma_0 \approx 2 \times 10^{-16}$ cm^2 from observations of the ζ Per cloud by van Dishoeck and Black (1982). Quantum mechanical calculations of the C_2–H_2 rotational excitation cross sections have subsequently been performed by Chambaud *et al.* (1988, as quoted by Le Bourlot, Roueff, and Viala 1987) and may differ by as much as factors of 2–3 from the values adopted here. Note that the uncertainty in σ_0 affects the absolute densities but not the relative values found for the various clouds. In the absence of any detailed information on the new cross sections, we have continued to adopt $\sigma_0 \approx 2 \times 10^{-16}$ cm^2, together with $I_R = 1$, throughout the analysis.

III. RESULTS

Table 4 summarizes the main results of the observations. It lists the measured equivalent widths with estimated 2 σ errors and the inferred column densities of interstellar C_2, CH, and CN for the various lines of sight. In some cases, data of previous observations are included for completeness. For CH the equivalent width of the $R_2(1) = R_f(\frac{1}{2})$ blend is given. For C_2 and CN the equivalent widths of only one of the stronger lines in the spectrum—the $Q(2)$ line in the case of C_2 and the $R_1(0)$ line in the case of CN (unless specified otherwise)—are given. If no line was detected, 2σ upper limits on the equivalent widths are listed. Upper limits on the total C_2 column density for a line of sight were taken to be a factor of 5 times the upper limits on the column density in $J'' = 2$. The population distribution of C_2 in some clouds is uncertain, but the factor 5 is appropriate for clouds with a temperature $T \lesssim 50$ K and density $n = n(H) + n(H_2) \gtrsim 200$ cm^{-3}. More details for specific lines of sight will be given below.

a) HD 80077

The southern star HD 80077 is a very luminous supergiant which lies close to the open cluster Pişmiş 11 (Moffat and FitzGerald 1977; Knoechel and Moffat 1982; Steemers and van Genderen 1986). HD 80077 appears to be suffering mass loss and to be surrounded by a massive cloud of dust from which it may have originated. Its estimated distance is about 3.0 kpc. Strong interstellar C_2 lines were seen in the spectra of this star both at ESO and at Cerro Tololo, as illustrated in Figure 1. Fourteen lines of interstellar C_2 arising from lower rotational levels up to $J'' = 14$ can be identified in the higher resolution spectrum obtained at ESO. Most of these lines are also seen in the CTIO spectrum. Because of the lower resolution, the $Q(8)$ and $P(4)$ lines at 8773 Å, which are separated by only 6.77 km s^{-1}, are blended in the latter observations. The measured equivalent widths and the deduced C_2 column densities for the two sets of observations are presented in Table 5. A check on the reliability of the results within each set of measurements is provided by a comparison of the column densities derived from the P, Q, and R lines that arise in the same lower rotational level J''. As Table 5 shows, the agreement is generally good, except for the R lines that lie on the steep wing of the broad stellar H I Paschen 12 feature. Note that in both sets of data the $Q(4)$ line appears somewhat broader at the top than the other C_2 lines in the spectrum. As pointed out by Gredel and Münch (1986), this broad absorption is most likely due to a new diffuse interstellar absorption band that is coincident with the C_2 line. Its strength has been estimated to be $W_\lambda = 5$ mÅ and has been subtracted from the strength of the total $Q(4)$ feature. An important test of the instrumental performances is provided by comparing the results obtained at the two different telescopes. As Table 5 shows, the agreement in equivalent widths between the two measurements is good; the differences are generally well within the 2 σ error bars and are of the order of 10%, except for a few weak lines with $W_\lambda < 5$ mÅ. The radial velocities derived from the interstellar lines toward HD 80077 are also consistent: $V_{LSR} = 1.4 \pm 1.8$ km s^{-1} and $V_{LSR} = 2.0 \pm 1.0$ km s^{-1} for the CTIO and ESO data, respectively.

Figure 2 shows the relative theoretical population distributions (cf. van Dishoeck and Black 1982) in the form $-\ln[5N_{J''}/N_2(2J''+1)]$ as functions of the excitation energy $\Delta E_{J''}/k$ in K of level J'' with respect to $J'' = 2$, for $T = 25$ K and $n\sigma_0/I_R$ ranging between 10^{-14} and 10^{-13} cm^{-1}. The dashed line indicates the thermal population distribution at $T = 20$ K. The observed C_2 rotational populations are included in the figure, and they agree well with theory for $n\sigma_0/I_R \approx 5 \times 10^{-14}$ cm^{-1}. If $I_R \approx 1$ and $\sigma_0 \approx 2 \times 10^{-16}$ cm^2 is adopted, the density in the HD 80077 cloud is $n \approx 250$ cm^{-3}, so that $n_H = n(H) + 2n(H_2) \approx n + n(H_2) \approx 500$ cm^{-3}, if most hydrogen is in molecular form in the cloud.

Figure 3 shows part of the CN (2, 0) band spectrum obtained at ESO. These measurements constitute the first detection of the red system of CN in interstellar clouds (van Dishoeck and Black 1984, 1985; Crutcher and Lutz 1985). The strongest CN line is the $R_1(0)$ line, which can clearly be identified in the spectrum. In addition, the weaker $^SR_{21}(0)$ and $R_1(1)$ lines can be measured, while the $^SR_{21}(1)$ line and the $^RQ_{21}(1)$ and $R_2(1)$ blend can be seen marginally. The strong $Q_1(1)$ and $^QR_{12}(1)$ blend is lost in an atmospheric feature, as is the $^QP_{21}(1)$ and $Q_2(1)$ blend. The spectrum of HD 80077 in the region of the (1, 0) band around 9140 Å was obtained at CTIO; unfortunately, all strong interstellar CN lines toward HD 80077 coincided with telluric H_2O lines at the time of the observations so that no reliable equivalent widths could be derived.

Table 6 lists the measured equivalent widths and deduced CN column densities. The total column density in the lowest

TABLE 4

SUMMARY OF OBSERVATIONS

		C_2			CN			CH				
STAR	$E(B-V)$	W_λ[a] (mÅ)	N[b] (10^{13} cm^{-2})	Telescope[c]	W_λ[d] (mÅ)	N[b] (10^{13} cm^{-2})	Telescope[c]	W_λ[e] (mÅ)	N[b] (10^{13} cm^{-2})	Telescope[c]	$v_\odot$[f] (km s^{-1})	v_{LSR}[f] (km s^{-1})
JM-1	1.69	≤5	≤7	CT	...	...	...	...	...	...	...	...
HDE 290861	1.25	≤6	≤8	CT	...	See text	...	...	...	...	...	...
HD 63804	1.19	(17 ± 4)	(17 ± 6)	ESO	(4.1 ± 2.0)	(3.6 ± 1.5)	ESO	...	...	...	+(38 ± 3)	+(20 ± 3)
HD 75149	0.41	<1.5	<2.2	ESO	...	...	...	(14.3 ± 0.6)[g]	(1.7 ± 0.3)[g]	ESO	+(21 ± 1)	+(5 ± 1)
HD 78344	1.40	(4.4 ± 2)	(8 ± 3)	CT	≤3	≤1	CT	...	...	...	+(25 ± 3)	+(9 ± 3)
HD 80077	1.52	(11.7 ± 1.2)	(13.5 ± 1.5)	ESO, CT	(6.8 ± 1.0)	(4.0 ± 0.6)	ESO	(45 ± 3)	(11 ± 2)	ESO	+(17 ± 2)	+(2 ± 2)
HD 80558	0.62	<3	<4.5	ESO	...	...	...	...	...	...	...	...
HD 92693	1.02	1.3:	(2.0 ± 1.0)	ESO	...	...	...	...	...	...	−(13 ± 2)	−(25 ± 2)
HD 94413	0.81	(9.2 ± 2)	(7 ± 2)	CT	(4.4 ± 2.0)	(5.7 ± 2.0)	CT	...	...	...	+(15 ± 3)	+(4 ± 3)
HD 94910	0.55:	<10	<15	ESO	...	...	...	...	...	...	...	...
HD 97300	0.44	<4	<6	CT	...	...	...	...	...	...	...	...
HD 106391	0.92	(8 ± 3)	(11 ± 3)	CT	(6 ± 3)	(2 ± 1)	CT	...	...	...	+(46 ± 3)	+(37 ± 3)
Wray 977	1.9	6:	8:	CT	...	...	...	...	...	...	−(20 ± 3)	−(29 ± 3)
HD 110432	0.52	(1.6 ± 0.3)	(3.0 ± 1.0)	ESO	(0.8 ± 0.4)	(0.5 ± 0.3)	ESO	(12.3 ± 0.5)	(1.5 ± 0.3)	ESO	+(8 ± 2)	+(1 ± 2)
HD 112272	1.05	<3	<4.5	ESO	...	...	...	...	...	...	...	...
HD 113422	1.02	4:	6:	CT	...	...	...	...	...	...	−(14 ± 3)	−(20 ± 3)
HD 115842	0.52	<8	<12	ESO	...	...	...	(15.1 ± 1.5)[g]	(1.8 ± 0.3)[g]	ESO	...	...
HD 134959	1.20	<4.5	<6.5	ESO	...	...	...	...	...	...	...	...
CPD −57°7059	1.43	<6	<8	CT	...	...	...	...	...	...	...	...
HD 147084	0.74	(4.2 ± 0.5)	(5.5 ± 1.0)	ESO	(1.0 ± 0.2)	(0.6 ± 0.2)	ESO	(29 ± 3)	(5 ± 1)	ESO	−(7 ± 1)	+(3 ± 1)
HD 147889	1.09	(10.1 ± 0.6)[h]	(12.0 ± 3.0)[h]	ESO	...	(0.4 ± 0.1)[i]	KP	(38 ± 3)	(10 ± 3)	ESO	−(7 ± 1)	+(3 ± 1)
Elias 16	2.1	<10	<15	CT	...	...	...	...	...	...	...	...
HD 148379	0.69	<1.0	<1.5	ESO	...	...	...	...	...	...	...	...
HD 152235	0.77	<6	<8	ESO	...	...	...	...	...	...	...	...
HD 152236	0.66	(1.2 ± 0.5)	(1.6 ± 0.6)	ESO	...	...	...	...	...	...	...	...
HD 154368	0.82	(5.2 ± 0.4)[h]	(5.8 ± 0.6)[h]	ESO	(5.0 ± 1.0)	(3.5 ± 0.5)	ESO	(36 ± 2)	(8 ± 2)	ESO	−(2.7 ± 0.5)	+(5.2 ± 0.5)
HD 156738	1.18	<6	<8	CT	...	...	...	(18 ± 6)	(3 ± 1)	MMT	+8	+16
HD 157038	0.89	<2	<3	CT	...	...	...	...	...	...	...	...
HD 160529	1.23	<2	<3	ESO	...	...	...	...	...	...	...	...
HD 166734	1.41	<4	<6	CT	...	...	...	(42 ± 5)[j]	(9 ± 1)[j]	MMT	...	...
HD 168607	1.60	<4	<6	ESO	...	...	...	(50 ± 4)	(14 ± 4)	MMT	+(22 ± 5)	+(36 ± 5)
BD −14°5037	1.57	(7.3 ± 2)	(6 ± 2)	ESO	...	...	...	(61 ± 4)[j]	(13 ± 5)[j]	MMT	Double[k]	Double[k]
HD 169454	1.14	(6.6 ± 0.8)	(7.0 ± 1.4)	ESO	(8.0 ± 0.6)	(5.5 ± 0.6)	ESO	(27 ± 2)	(5.8 ± 0.8)	MMT	−(9 ± 2)	+(5 ± 2)
HD 169754	1.31	<8	<12	ESO	...	...	...	(41 ± 4)	(8 ± 1)	MMT	...	...
HD 181615	?	<4	<6	ESO	...	...	...	...	...	...	...	...
HDE 229059	1.7	...	...	...	...	...	...	(57 ± 6)	(23 ± 14)	MMT	+(4 ± 5)	+(21 ± 5)
BD +66°1675	1.4	[l]	(21 ± 12)[l]	...	...	...	...	(72 ± 8)[m]	(15 ± 5)[m]	MMT	Double[m]	Double[m]

[a] Equivalent width of C_2 $Q(2)$ line.
[b] Total C_2, CN, or CH column density.
[c] Telescope at which observations were performed.
[d] Equivalent width of CN (2, 0) $R_1(0)$ line for ESO data; for CTIO data see text.
[e] Equivalent width of CH $A\,^2\Delta$–$X\,^2\Pi$ (0, 0) $R_2(1)$ blend at 4300.3 Å.
[f] Average velocity of the C_2, CH, and CN lines.
[g] Danks, Federman, and Lambert 1984.
[h] van Dishoeck and de Zeeuw 1984.
[i] Crutcher and Chu 1985.
[j] Probably multiple components; column density is total for a two-component fit of the profile.
[k] Two components visible in spectra of Gredel and Münch 1986; column densities are for both components.
[l] C_2 column density from Lutz and Crutcher 1983, adjusted for the adopted oscillator strength.
[m] The CH line shows two distinct velocity components; the equivalent width and column density are sums for both components.

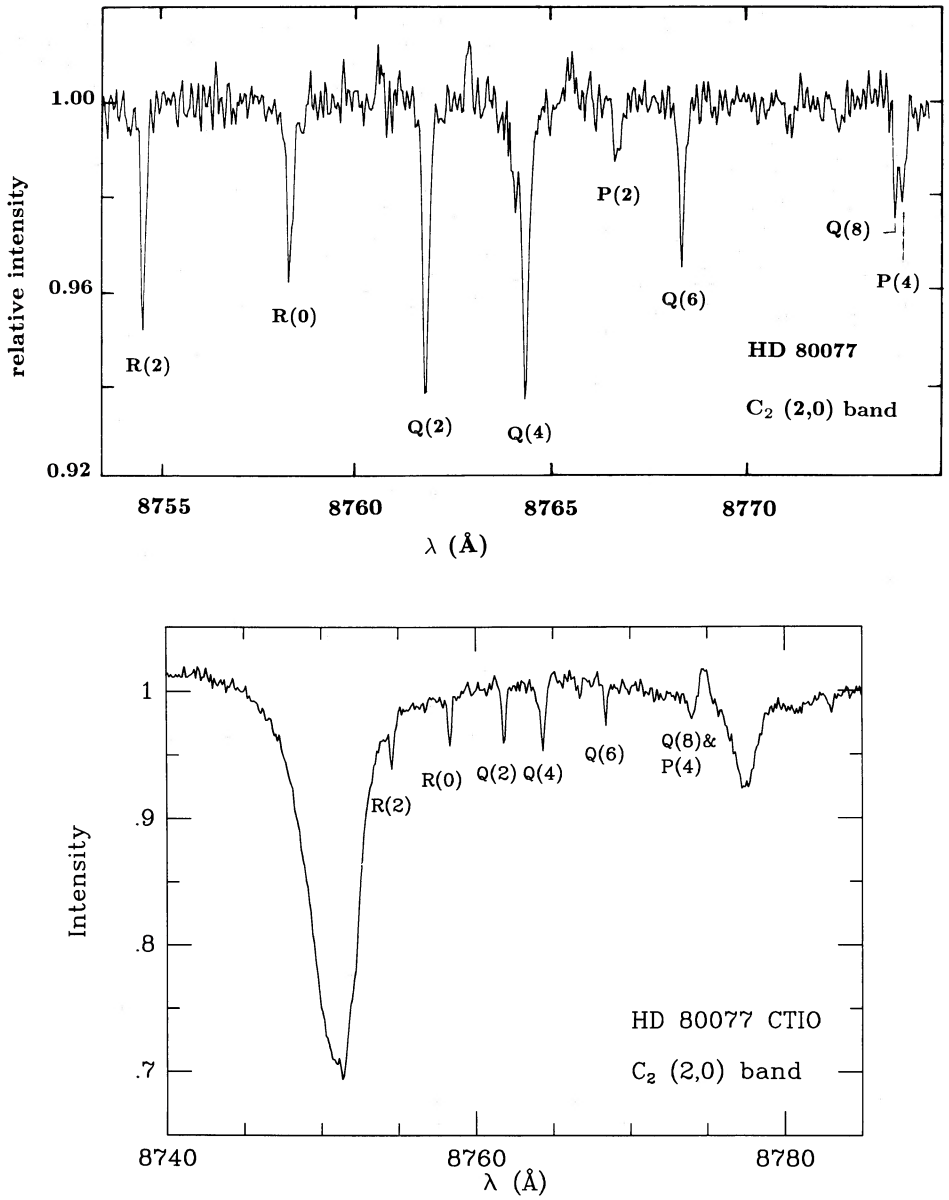

FIG. 1.—Spectra in the region of the C_2 (2, 0) Phillips band of HD 80077. *Top:* rectified spectrum obtained at ESO from which the broad stellar H I Paschen 12 feature has been removed; *bottom:* spectrum obtained at CTIO including the stellar line. Various interstellar C_2 lines are indicated. In these and all subsequent spectra, the abscissa indicates wavelength with respect to a laboratory frame.

level $N'' = 0$, $J'' = 1/2$ is $(3.0 \pm 0.4) \times 10^{13}$ cm^{-2}, and the best estimates of the column density in the excited $N'' = 1$, $J'' = 3/2$ and 1/2 levels are $(7 \pm 4) \times 10^{12}$ cm^{-2} and $(3 \pm 2) \times 10^{12}$ cm^{-2}, respectively. The column densities in the excited levels are uncertain because some important lines are lost in the atmospheric features. Nevertheless, they are consistent with an excitation temperature $T_{ex} = 2.5 \pm 0.8$ K controlled by the 2.7 K microwave background radiation.

Interstellar CH was detected toward HD 80077 with the ESO CAT telescope equipped with the CCD detector (C. P. de Vries 1987, private communication). The inferred CH column density in the optically thin limit is 5.4×10^{13} cm^{-2}, and increases to 1.1×10^{14} cm^{-2} if b is as small as 1 km s^{-1}.

b) HD 169454

HD 169454 is another bright supergiant that has a significant amount of molecular material in front of it. Figure 4 shows the rectified spectrum of HD 169454 in the region of the C_2 lines obtained at ESO (see also van Dishoeck and Black 1984). Nine lines of interstellar C_2 arising from lower rotational levels up to $J'' = 10$ have been identified in the spectrum. The measured equivalent widths and column densities are collected in Table 7. Also included in the table are the equivalent widths measured recently for the same line of sight by Gredel and Münch (1986) with the same telescope and detector. Although the total integration time of the latter observations

TABLE 5

COMPARISON OF OBSERVATIONS OF INTERSTELLAR C_2 TOWARD HD 80077

LINE	W_λ (mÅ)		$N_{J''}$ (10^{13} cm^{-2})	
	ESO[a]	CTIO[a]	ESO	CTIO
$R(0)$	9.4	10.1	1.4	1.5
$P(2)$	2.8	3.6	4.1	5.3
$Q(2)$	11.7	12.3	3.5	3.6
$R(2)$	10.8	12.0	4.0	4.4
$P(4)$	3.6	4.2[b]	3.2	3.7
$Q(4)$	17.2[c]	19.0[c]	3.6	4.1
$R(4)$	...	11.7	...	5.1
$P(6)$	1.0	2.8	0.8	2.1
$Q(6)$	6.2	7.2	1.8	2.1
$R(6)$	4.4	...	2.1	...
$P(8)$	1.4	1.4	1.0	1.0
$Q(8)$	3.4	2.0[b]	1.0	0.6
$Q(10)$	2.3	1	0.7	0.3
$R(10)$	1.0:	2.0	0.5	1.0
$Q(12)$	1.5	1	0.4	0.3
$Q(14)$	1.2	...	0.3	...
Total observed[d]	...	...	12.7	13.4
Total[e]	...	...	13.5	14.7

[a] The uncertainty in the equivalent widths is 0.5–1.0 mÅ for both sets of observations.

[b] The $Q(8)$ and $P(4)$ lines are blended in the CTIO observations; the decomposition is based upon a two-component, least-squares fit of Gaussian profiles.

[c] Including a possible underlying diffuse band. An equivalent width of 5 mÅ has been subtracted to determine the column density.

[d] Total column density summed over all observed levels.

[e] Total column density including the contribution of unobserved levels according to the best-fitting model.

was somewhat longer than that in the present work, the two sets of measurements agree reasonably well. The largest discrepancy occurs for the $R(0)$ line. The heliocentric radial velocity $V_\odot = -7.1 \pm 1.0$ km s^{-1} obtained in this work is just consistent with $V_\odot = -8.5 \pm 0.6$ km s^{-1} found by Gredel and Münch (1986), but differs from the velocities found for the strong atomic K I lines toward HD 169454: one component at $V_\odot = -9.6$ km s^{-1} according to Herbig and Soderblom (1982) or two components at $V_\odot = -12.1$ and $+4.8$ according to Chaffee and White (1982).

TABLE 7

INTERSTELLAR C_2 OBSERVATIONS TOWARD HD 169454

LINE	W_λ (mÅ)		$N_{J''}$ (10^{13} cm^{-2})	
	This Work	GM[a]	This Work	GM
$R(0)$	(5.6 ± 1.0)	8.2	(0.8 ± 0.2)	1.2
$P(2)$	(1.3 ± 0.3)	2.3	(1.9 ± 0.4)	3.4
$Q(2)$	(6.6 ± 0.8)	8.0	(1.9 ± 0.3)	2.4
$R(2)$	(6.0 ± 0.5)	6.1	(2.2 ± 0.3)	2.3
$P(4)$	(1.7 ± 0.8)	2.0	(1.5 ± 0.7)	1.8
$Q(4)$	(7.9 ± 0.7)[b]	5.0	(1.7 ± 0.3)	1.5
$R(4)$	...	3.8	...	1.7
$P(6)$	<1.5	1.9	<1.1	1.5
$Q(6)$	(3.9 ± 0.5)	3.1	(1.1 ± 0.2)	0.9
$Q(8)$	(1.5 ± 0.5)	2.6	(0.4 ± 0.2)	0.7
$Q(10)$	(1.0 ± 0.8)	1:	(0.3 ± 0.2)	0.3:
$Q(12)$	<1.5	1:	<0.4	0.3:
Total observed[c]	...	...	6.2	7.3
Total[d]	...	...	7.0	7.8

[a] Gredel and Münch 1986.

[b] Including a possible contribution of $W_\lambda \approx 2$ mÅ due to a diffuse interstellar band. This contribution has been removed in the calculation of the column density.

[c] Total column density summed over all observed levels.

[d] Total column density including the contribution of unobserved levels according to the best-fitting model.

The measured C_2 rotational population distributions have been compared with the theoretical population distributions in the same way as illustrated for the case of HD 80077 in Figure 2. The relative populations of the $J'' = 0$ and 2 levels clearly suggest a low temperature in the cloud, $T = 15^{+10}_{-5}$ K. The populations of the higher rotational levels are compatible with $n\sigma_0/I_R \approx 6 \times 10^{-14}$ cm^{-1} corresponding to $n \approx 300$ cm^{-3}, if $I_R \approx 1$ and $\sigma_0 \approx 2 \times 10^{-16}$ cm^2 are assumed.

In Figure 5 the spectrum of HD 169454 in the region of the CN A–X (2, 0) band is presented. The spectrum clearly shows all three interstellar lines originating from the lowest CN rotational level $N'' = 0$, $J'' = 1/2$. The measured equivalent widths are included in Table 6. The inferred column density in $N'' = 0$, $J'' = 1/2$ is $(3.8 \pm 0.5) \times 10^{13}$ cm^{-2}. Lines originating from the excited rotational levels $N'' = 1$, $J'' = 1/2$ and 3/2 have also been identified in the spectrum. The measured strengths of the

TABLE 6

OBSERVATIONS OF THE INTERSTELLAR CN (2, 0) RED SYSTEM TOWARD VARIOUS STARS

LINE	HD 80077		HD 169454		o Sco		HD 154368	
	W_λ[a]	$N_{J''}$[b]	W_λ	$N_{J''}$	W_λ	$N_{J''}$	W_λ	$N_{J''}$
$R_1(0)$	(6.8 ± 1.0)	$(3.1 \pm 0.4)(13)$	(8.0 ± 0.6)	$(3.6 \pm 0.3)(13)$	(1.0 ± 0.2)	$(4.5 \pm 1.0)(12)$	(5.0 ± 1.0)	$(2.4 \pm 0.4)(13)$
$^RQ_{21}(0)$	Atm[c]	...	(5.9 ± 0.6)	$(4.2 \pm 0.5)(13)$	(0.65 ± 0.2)	$(4.7 \pm 1.4)(12)$	(3.1 ± 0.8)	$(2.3 \pm 0.6)(13)$
$^SR_{21}(0)$	(1.7 ± 0.6)	$(2.9 \pm 1.2)(13)$	(2.4 ± 0.6)	$(4.1 \pm 1.2)(13)$	<0.3	$<5.2(12)$	(1.2 ± 0.8)	$(2.1 \pm 1.4)(13)$
$Q_1(1) + {}^QR_{12}(1)$[d]	Atm	...	Atm	...	<0.3	$<2(12)$	(2.5 ± 0.8)	$(2.0 \pm 0.7)(13)$
$Q_2(1) + {}^QP_{21}(1)$[d]	Atm	...	<2.5	$<4(13)$	Atm	...	(1.1 ± 0.8)	$(1.6 \pm 1.0)(13)$
$R_2(1) + {}^RQ_{21}(1)$[d]	0.5:	0.5(13):	(1.7 ± 0.6)	$(1.8 \pm 0.6)(13)$	<0.3	$<3(12)$	0.5:	0.5(13):
$R_1(1)$	(1.0 ± 0.6)	$(0.7 \pm 0.4)(13)$	(1.6 ± 0.6)	$(1.1 \pm 0.5)(13)$	Atm	...	<1.6	$<1.1(13)$
$^SR_{21}(1)$	0.4:	0.8(13):	...	...	<0.3	$<6(12)$	0.8:	1.6(13)

[a] In mÅ.

[b] In cm^{-2}.

[c] Atm = interstellar line lost in atmospheric feature.

[d] Unresolved blend; the inferred column density refers to the sum of that in $J'' = 1/2$ and 3/2.

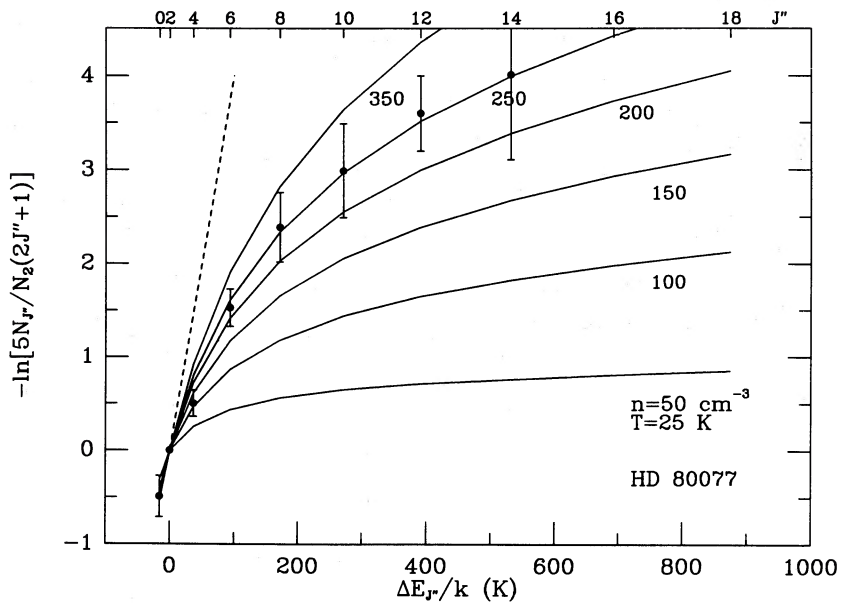

FIG. 2.—Observed rotational populations of C_2 relative to that of $J'' = 2$ for the cloud in front of HD 80077. The solid lines indicate the theoretical distributions at a kinetic temperature $T = 25$ K and various densities, assuming $I_R = 1$ and $\sigma_0 = 2 \times 10^{-16}$ cm^2. The dashed line is the thermal distribution at $T = 25$ K.

lines result in a column density in $N'' = 1$, $J'' = 3/2$ of $(1.1 \pm 0.3) \times 10^{13}$ cm^{-2}, and in $N'' = 1$, $J'' = 1/2$ of $(0.6 \pm 0.2) \times 10^{13}$ cm^{-2}. The observed column densities in the excited levels yield an excitation temperature $T_{ex} = 2.9 \pm 0.4$ K.

Interstellar CH has been observed toward HD 169454 with the MMT. The deduced CH column density is 2.9×10^{13} cm^{-2} for an optically thin line, and increases to 5.8×10^{13} cm^{-2} if b is as small as 0.5 km s^{-1}.

The molecular cloud in front of HD 169454 has recently been investigated in much more detail by Jannuzi *et al.* (1988) through CO millimeter line observations, and appears to be a good example of an isolated translucent cloud. The map of CO emission shows three large condensations and evidence of unresolved structure on smaller scales. The line of sight to HD 169454 passes fortuitously almost through the peak of the CO emission in one of the clumps. The inferred CO column density in the direction of the star is (1–9) $\times 10^{16}$ cm^{-2} at $V_{LSR} = 6.0 \pm 0.2$ km s^{-1}. The width of the ^{13}CO line suggests $b \approx 0.5$ km s^{-1}, the value adopted in the analysis of the CH line.

c) *HD 147084 (o Sco)*

The star *o* Sco lies near the southern part of the Ophiuchus complex, about 87′ (4 pc) in projection away from the core of

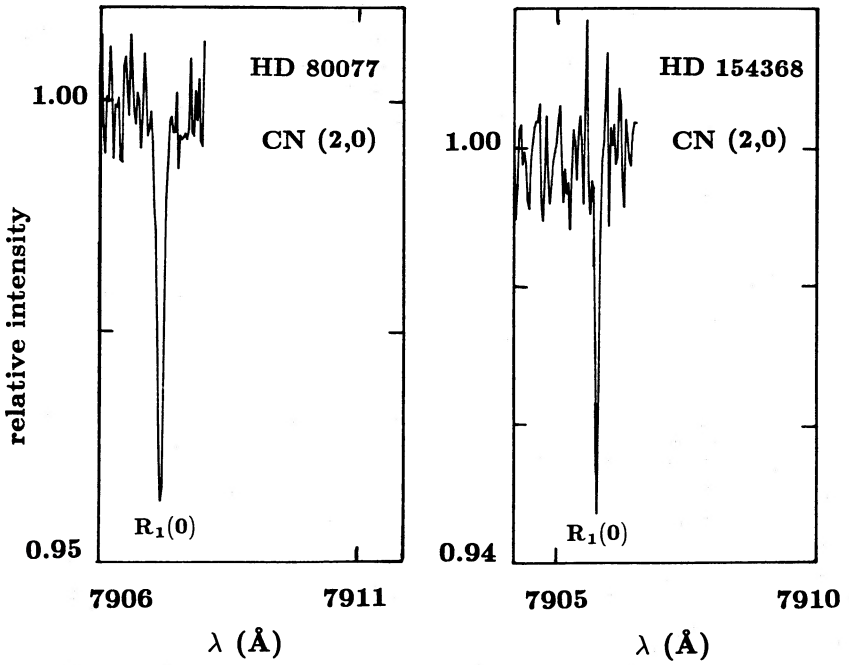

FIG. 3.—Observed $R_1(0)$ line in the (2, 0) band of the red system of interstellar CN toward HD 80077 and HD 154368 around 7900 Å. The spectra were obtained at ESO.

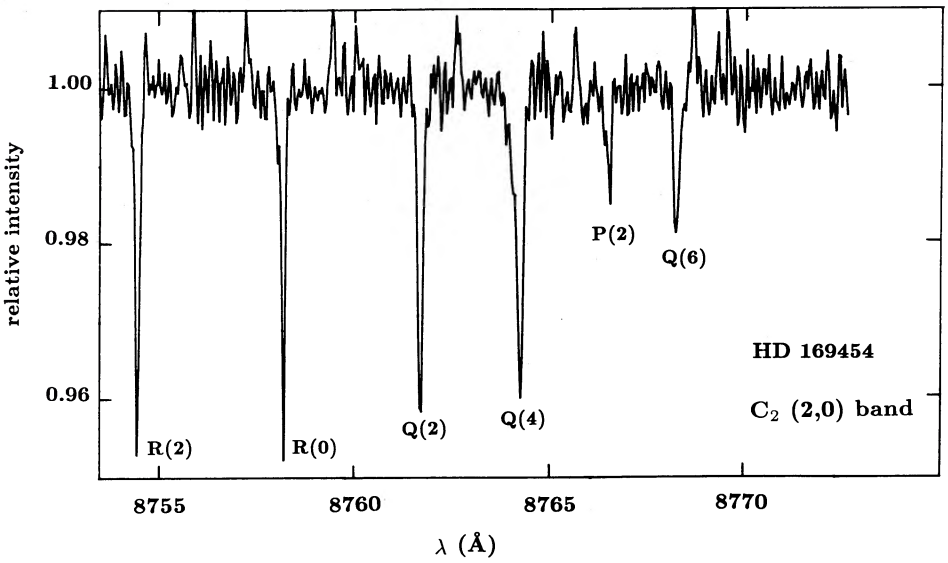

FIG. 4.—Spectrum of HD 169454 in the region of the C_2 (2, 0) Phillips band obtained at ESO

the ρ Oph molecular cloud. In contrast with the other stars in our sample, this star is not an early O or B star but one of later spectral type, A5 II. In Figure 6 the rectified spectrum of o Sco in the region of the C_2 lines is presented. As is apparent from the spectrum, o Sco is a slow rotator with $v \sin i \approx 7$ km s^{-1}, and many comparatively sharp stellar features interfere with the interstellar C_2 lines. C_2 lines up to the $Q(14)$ line are indicated in the figure. Fortunately, only the C_2 $Q(4)$, $P(2)$, and $P(8)$ lines were lost in the stellar lines. The measured equivalent widths and column densities are listed in Table 8. The average heliocentric radial velocity of the C_2 lines is $V_\odot = -7.3 \pm 1$ km s^{-1}, corresponding to $V_{LSR} = 2.8 \pm 1$ km s^{-1}. The latter velocity is in good agreement with $V_{LSR} = 2.5$–4.0 km s^{-1} found in millimeter CO observations in the Ophiuchus cloud in general (Encrenaz, Falgarone, and Lucas 1975).

The observed C_2 rotational population appears to be consistent with $T \approx 40$ K and $n\sigma_0/I_R \approx 4 \times 10^{14}$ cm^{-1}, or $n \approx 200$ cm^{-3}, if $I_R \approx 1$ and $\sigma_0 = 2 \times 10^{-16}$ cm^2. In fact, the C_2 rotational distribution in the o Sco cloud is very similar to that found toward other stars in the Ophiuchus region, such as ζ Oph, ρ Oph, and in particular χ Oph (van Dishoeck and de Zeeuw 1984; Danks and Lambert 1983; van Dishoeck 1984). The kinetic temperature, which is sensitive to an uncertain $R(0)$ equivalent width, is not well constrained and may range between 35 and 80 K.

Lines in the red system of interstellar CN have also been detected toward o Sco. The lines are weak, however, as Table 6 shows: even the $R_1(0)$ line has an equivalent width of only 1 mÅ. No lines originating in excited rotational levels with $N'' = 1$ are detected. The upper limits on the column densities in these levels are consistent with an excitation temperature $T_{ex} < 3.2$ K. The total CN column density listed in Table 6 is obtained under the assumption that $T_{ex} = 2.7$ K.

In contrast with the CN lines, the interstellar CH line

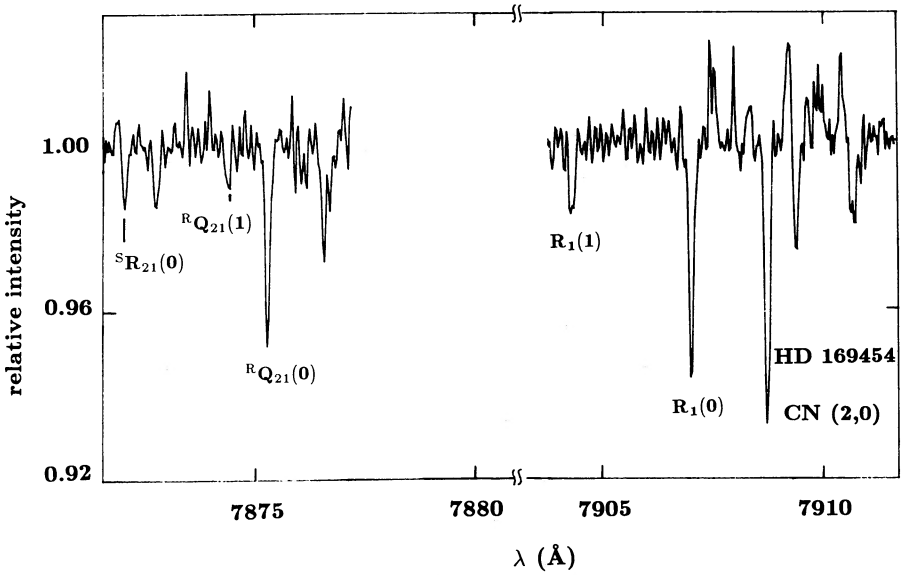

FIG. 5.—Spectrum of HD 169454 in the region of the CN (2, 0) red system band obtained at ESO. The lines that have not been designated are due to telluric features.

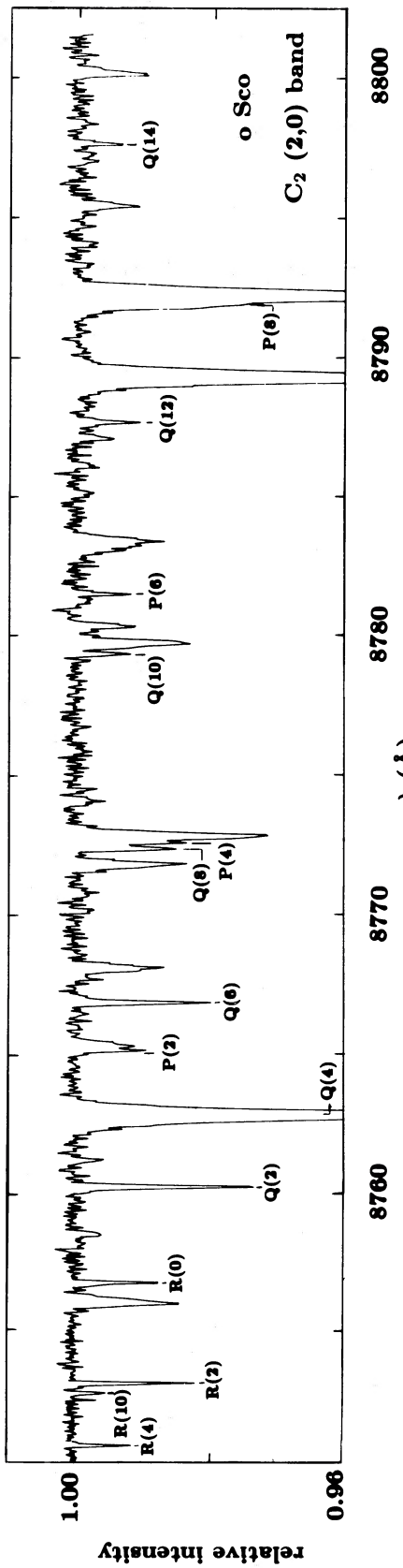

FIG. 6.—Spectrum of *o* Sco in the region of the C_2 (2, 0) Phillips band obtained at ESO, with the various C_2 lines identified. The lines that have not been designated are narrow stellar features.

TABLE 8

OBSERVATIONS OF INTERSTELLAR C_2 TOWARD VARIOUS STARS

LINE	o Sco		HD 110432		HD 78344		HD 94413		HD 152236	
	W_λ[a,b]	$N_{J''}$[c]	W_λ[a,b]	$N_{J''}$[c]	W_λ[a,b]	$N_{J''}$[c]	W_λ[a,b]	$N_{J''}$[c]	W_λ[a,d]	$N_{J''}$[c]
R(0)	1.8	2.7(12)	1.5:	2(12):	4.7	6.9(12)	5.4	8.0(12)	0.7	1.0(12)
P(2)	1.1	1.6(13)	...	...	<2	≤3(13)	<2	≤3(13)	...	...
Q(2)	4.2	1.2(13)	1.6	4.7(12)	4.4	1.3(13)	9.2	2.7(13)	1.2	3.5(12)
R(2)	2.1	0.8(13)	0.4:	1.5(12):	4.2	1.5(13)	3.7	1.4(13)	1.0	3.7(12)
P(4)	2.1	1.9(13)	0.7:	6(12):	<4	<3.5(13)	<2	<1.8(13)	...	...
Q(4)	St[e]	...	1.0	2.9(12)	7.9	2.3(13)	3.3	1.0(13)	0.9	2.6(12)
R(4)	1.7	0.8(13)	<1.5	<6(12)	5.3	2.3(13)	4.7	2.1(13)	...	...
P(6)	0.8	6.1(12)	0.5:	4(12):	<4	<3(13)	2.1	1.6(13)	...	...
Q(6)	2.9	8.5(12)	2.0	5.9(12)	3.0	8.8(12)	<3	<0.9(13)	1.0	2.9(12)
R(6)	...	...	1.2	5.8(12)	3.4	1.6(13)	4.2	2.0(13)	...	...
Q(8)	2.7	7.9(12)	1.0:	3(12):	2.6[f]	7.6(12)?	1.8[f]	3.0(12)	<0.7	<2(12)
R(8)	...	...	0.8:	4(12):	1.7	8.5(12)	<3	<1.5(13)	...	...
Q(10)	1.2	3.5(12)	1.5:	4(12):	1.7	5.0(12)	<3	<9(12)	...	...
R(10)	0.6	3.1(12)	...	...	...	...	...	...	...	...
Q(12)	1.2	3.5(12)	...	...	...	...	...	...	...	...
R(12)	0.5:	3(12)	...	...	...	...	...	...	...	...
Q(14)	0.8	2.3(12)	...	...	...	...	...	...	...	...
Total observed[g]	...	5.0(13)	...	2.2(13)	...	6.6(13)	...	6.0(13)	...	1.0(13)
Total[h]	...	5.5(13)	...	3.0(13)	...	7.9(13)	...	6.7(13)	...	1.6(13)

[a] Equivalent width in mÅ.
[b] The uncertainty in W_λ is about 2 mÅ.
[c] Column density in cm^{-2}.
[d] The uncertainty in W_λ is about 0.5 mÅ.
[e] St = interstellar line lost in a stellar feature.
[f] Including a contribution of at least 1 mÅ from the P(4) line.
[g] Total column density summed over all observed levels.
[h] Total column density including the contribution of unobserved levels according to the best-fitting model.

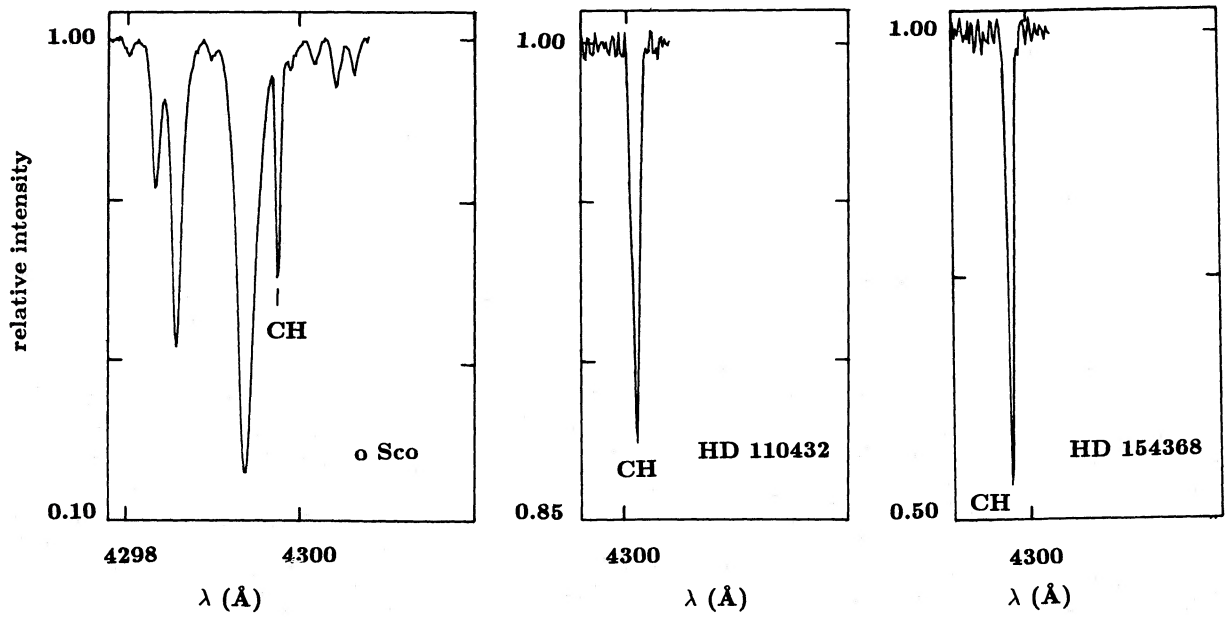

FIG. 7.—Observed CH A–X interstellar lines toward o Sco, HD 110432, and HD 154368 obtained at ESO

toward *o* Sco is very strong. As Figure 7 illustrates, the interstellar CH line at 4300 Å lies on the wing of a stellar feature, so that the measured strength is somewhat uncertain. The high spectral resolution is crucial for separating the stellar and interstellar features in this wavelength range. The deduced CH column density is 3.5×10^{13} cm^{-2} for an unsaturated line, and increases to 5×10^{13} cm^{-2} if b is as small as 1 km s^{-1}.

d) The Coalsack Region

The southern Coalsack region is one of the most prominent dust complexes in the southern sky. From optical star count measurements (Tapia 1973) the complex appears to be very irregular, with the extinction highly variable over small areas. The mean photometric distance to the cloud complex is about 175 pc (Rodgers 1960). Radio observations of H_2CO and OH (Brooks, Sinclair, and Manefield 1976) and CO in the $J = 1 \rightarrow 0$ (Huggins *et al.* 1977) and $J = 2 \rightarrow 1$ transitions (de Vries *et al.* 1984) have been performed for some globule-like regions. The Coalsack thus appears a promising place to search for molecular absorption lines.

Several bright, reddened stars have been identified in the Coalsack complex (cf. Table 1). Of the stars, HD 110432, which lies close (45′ or 2.3 pc) to one of the globules observed in molecular lines at radio wavelengths, appears to be the best candidate for optical absorption-line observations. The spectrum of HD 110432 has been studied extensively at ultraviolet wavelengths using the *IUE* satellite (Codina *et al.* 1984). Although the primary aim of that study was to search for absorption lines of highly ionized species indicative of mass loss of the star, the spectra also clearly showed atomic and molecular absorption lines of interstellar origin. The distance to the star was found to be 430 ± 60 pc, thus placing it well behind the Coalsack.

Lines of interstellar C_2 have been detected toward HD 110432 at ESO. However, as Table 8 shows, the measured equivalent widths and inferred column densities are small compared with those for other highly reddened lines of sight. The C_2 data toward HD 110432 are not good enough to permit an accurate determination of the physical conditions in the cloud. The $J'' = 0/J'' = 2$ population ratio suggests a very low temperature, $T \lesssim 20$ K in the cloud, in harmony with the radio observations (Brooks, Sinclair, and Manefield 1976). The comparatively high populations in $J'' = 6$–8 indicate a relatively low density $n \lesssim 200$ cm^{-3}, for a normal near-infrared radiation field $I_R \approx 1$ and $\sigma_0 = 2 \times 10^{-16}$ cm^2.

Only one very weak line of interstellar CN with an equivalent width less than 1 mÅ has been detected in the spectrum of HD 110432 at the same velocity as that of the C_2 lines. The inferred CN column density, obtained under the assumption of an excitation temperature of 2.7 K, is $(5 \pm 2.5) \times 10^{12}$ cm^{-2}. Interstellar CH has clearly been detected toward HD 110432 (cf. Fig. 7), although the strength of the 4300 Å line is less than one-third of that toward other stars, resulting in a column density of $(1.5 \pm 0.3) \times 10^{13}$ cm^{-2}. In fact, the C_2, CH, and CN column densities are all more like those found in the classical diffuse molecular clouds with $E(B-V) \approx 0.3$ mag, such as the ζ Per and ζ Oph clouds, than like those in translucent or dark clouds. A very uncertain estimate of the CO column density from the *IUE* ultraviolet observations toward this star gives $N(CO) \approx (0.5$–$2) \times 10^{15}$ cm^{-2} (Codina *et al.* 1984), similar to that found in some classical diffuse clouds.

The C_2, CH, and CN lines occur at a heliocentric radial velocity of $V_\odot = 8 \pm 2$ km s^{-1}, which corresponds to $V_{LSR} = 0 \pm 2$ km s^{-1}. These velocities differ somewhat from the velocities $V_{LSR} = -4$ to -7 km s^{-1} found in the radio observations of atomic hydrogen (Bowers, Kerr, and Hawarden 1980) and of various molecules.

Quite disappointingly, none of the other more highly reddened lines of sight in the Coalsack studied at ESO showed any detectable interstellar C_2 lines. Some weak lines which can be ascribed to C_2 have been observed in the spectrum of HD 113422 obtained at CTIO, but these are marginal detections at best. The measured equivalent widths and resulting column densities are included in Table 4. The possible C_2 lines occur at a velocity $V_{LSR} = -20 \pm 1$ km s^{-1}, which is very different from that found from the radio molecular observations in the Coalsack region.

e) HD 154368

Interstellar C_2 has been detected toward the southern star HD 154368 by van Dishoeck and de Zeeuw (1984). As illustrated by Blades and Bennewith (1973), the star lies in a region of extensive obscuration near the Galactic equator. The measured C_2 rotational population suggests $T \approx 25$ K and $n \approx 225$ cm^{-3}, corresponding to $n_H \approx 350$ cm^{-3}. The inferred C_2 column density corrected for the smaller oscillator strength adopted here is 5.8×10^{13} cm^{-2}.

Several lines in the red system of interstellar CN are detected in the present observations, which are summarized in Table 6. The strongest $R_1(0)$ line is illustrated in Figure 3. The column density in the lowest level $N'' = 0$, $J'' = 1/2$ is relatively well established to be $(2.3 \pm 0.5) \times 10^{13}$ cm^{-2}. The column densities in the upper levels $N'' = 1$, $J'' = 3/2$ and 1/2 are more uncertain, $(1.3 \pm 0.4) \times 10^{13}$ and $(0.6 \pm 0.2) \times 10^{13}$ cm^{-2}, respectively, and suggest an excitation temperature $T_{ex} = 4.2 \pm 1.5$ K that is possibly somewhat in excess of the 2.7 K background radiation. The total CN column density is $(4.2 \pm 0.7) \times 10^{13}$ cm^{-2}.

The results for the CN red system can be compared with those for the violet system obtained by Blades (1978), and more recently by Meyer and Hawkins (1987). Although the measured equivalent widths in the latter study are very accurate, the inferred column densities are uncertain due to the strong saturation of the $R(0)$ line. For any Doppler parameter $b \geq 1$ km s^{-1}, the inferred column density in the lowest $N'' = 0$ level from the data of Meyer and Hawkins is less than 1.3×10^{13} cm^{-2}, which is almost a factor of 2 below that inferred from the red system observations. This would suggest either that the adopted oscillator strength for the red system is too low by a factor of about 2, or that the appropriate Doppler parameter b is approximately 0.7 km s^{-1}. A larger oscillator strength for the CN red system would be consistent with the theoretical calculations of Larsson, Siegbahn, and Ågren (1983), but not with the experimental values and the newer calculations of Bauschlicher, Langhoff, and Taylor (1988). An estimate of the broadening of the molecular lines can be obtained from millimeter observations of other species in the cloud. In particular, the measurements of the CO $J = 2 \rightarrow 1$ emission of Lada and Blitz (1988) toward the star give a line width $\Delta V \approx 1.4$ km s^{-1}, corresponding to $b \approx 0.8$ km s^{-1}. This could be an upper limit on the value of b appropriate for the CN lines if the CO line is saturated or if the antenna beam averaged over velocity structure in the cloud. Observations of the ^{13}CO line profile in this direction would be useful. The effect of line saturation is such that the $N'' = 0$ column densities derived from the red and violet lines are in complete agreement at 2.3×10^{13} cm^{-2} for

$b = 0.65$ km s^{-1}. On the other hand, the excited state populations derived from the $P(1)$ and $R(1)$ lines of the violet system are in harmony for $b \approx 0.9$ km s^{-1}, and suggest a somewhat lower column density in $N'' = 1$, 1×10^{13} cm^{-2}, than is derived from the red system observations. Uncertainty about the line broadening therefore affects the determination of the rotational excitation temperature. If $b = 0.9$ km s^{-1}, the excitation temperature for the $N'' = 0$ and $N'' = 1$ levels is $T_{ex} = 3.6$ K (Meyer and Hawkins 1987); however, if $b = 0.65$ km s^{-1} and the unresolved line splittings in the violet system are taken into account, then the violet system data imply $T_{ex} = 2.7$ K. The former result would require substantial local excitation through collisions in a cloud at moderately high density, while the latter result would be in harmony with a low density like that suggested by the C_2 measurements with CN excitation determined only by the cosmic background radiation. In summary, the CN red system measurements, the low density inferred from the C_2 observations, and the existing CO emission-line data all suggest that the line width is small, although further observations will be required to resolve the issues of the uncertain red system oscillator strength and the amount of local excitation of CN.

It is usually ignored that the violet system lines are actually unresolved blends. For example, the (0, 0) $R(0)$ feature is, in fact, a blend of $R_1(0)$ and $^RQ_{21}(0)$ lines with relative strengths of $\frac{2}{3}$ and $\frac{1}{3}$, respectively. Although their true separation is not accurately known, it can be estimated to be 0.0035 Å (0.27 km s^{-1} in Doppler velocity) according to the spectroscopic constants of Engleman (1974). As long as the Doppler width is large compared with this line splitting, the doublet structure has a negligible effect on the curve of growth and saturation corrections. For very narrow lines, however, the doublet structure should be included in the analysis: at $b = 0.65$ km s^{-1} in the case considered here, for example, the line splitting in $R(0)$ has a 10% effect on the inferred column density. If the line width were as small as $b = 0.5$, then neglect of the unresolved structure would cause the derived $N'' = 0$ column density to be overestimated by a factor of 1.4.

The measured equivalent width of the CH line in this work is large (see Fig. 7) but is significantly less than that found by Blades (1978). The inferred CH column density is 4.3×10^{13} cm^{-2} in the optically thin limit, and increases to 8×10^{13} cm^{-2} for b as small as 0.8 km s^{-1}.

The wavelength shifts of the C_2, CH, and CN lines give $V_\odot = -2.7 \pm 0.5$ km s^{-1}, or $V_{LSR} = +5.2 \pm 0.5$ km s^{-1} for the absorbing cloud, consistent with $V_{LSR} = +5.5$ km s^{-1} measured for the CO millimeter emission (Lada and Blitz 1988).

f) Other Lines of Sight

The observations of interstellar C_2 for other lines of sight are summarized in Tables 4 and 8.

i) *HD 63804*

Several features which can plausibly be assigned to the $Q(2)$, $Q(4)$, and $Q(6)$ lines of interstellar C_2 have been discovered in the spectrum of HD 63804. The lines are broad, $\Delta v \approx 10$ km s^{-1}, and suggest a total column density $N(C_2) \approx (1.7 \pm 0.6) \times 10^{14}$ cm^{-2} for a temperature $T \approx 50$ K and $n \approx 350$ cm^{-3}. The broadening may be caused by blending of several components along the line of sight.

Narrow lines belonging to the red system of CN have been found in the spectrum of the star at the same velocity, $V_{LSR} \approx 20$ km s^{-1}, as that of the C_2 lines. The column density in $N'' = 0$ is $(2.5 \pm 1.0) \times 10^{13}$ cm^{-2}, leading to an estimated total column density of $(3.6 \pm 1.5) \times 10^{13}$ cm^{-2}. No CH measurements have yet been performed for this star.

ii) *BD −14°5037 = SAO 161452*

The star BD −14°5037 is located in the Sct OB3 association only 40′ away from the luminous supergiant HD 169454 discussed in § III*b*. A few lines belonging to interstellar C_2 have been found in the spectrum of BD −14°5037 obtained after a 2 hr exposure. Spectra of much higher quality have been obtained by Gredel and Münch (1986), who integrated on the star for 14 hr with the same instrument. Their spectra show an interesting double structure with a velocity difference of about 10 km s^{-1}. The velocity of one of the components is close to that found for the HD 169454 cloud, suggesting that the absorption arises in an extension of the same cloud structure. Although the extent of the HD 169454 cloud as mapped in CO by Jannuzi *et al.* (1988) is smaller than the separation between the two stars, the Massachusetts–Stony Brook Galactic plane survey (Sanders *et al.* 1986; Clemens *et al.* 1986) shows a small isolated CO feature at the position of BD −14°5037 at the appropriate velocity. It is not known whether the two clouds are connected by more dilute molecular gas, although the large atomic cloud observed by Riegel and Crutcher (1972) covers both positions. The C_2 rotational excitation of this component toward BD −14°5037 as measured by Gredel and Münch indicates a somewhat higher temperature $T > 30$ K and a somewhat higher density $n \geq 400$ cm^{-3} than found toward HD 169454. The C_2 column densities are comparable in the two cases. The C_2 column density and excitation in the second component toward BD −14°5037 are similar to those of the first component (Gredel and Münch 1986).

Interstellar CH has been detected toward BD −14°5037 using the MMT. The velocity resolution of these observations is inadequate to separate the two components, but a single-component profile is unreasonably broad ($b \approx 10$ km s^{-1}, after correction for instrumental broadening), while a two-component fit to the profile is consistent with features separated by 12 km s^{-1}.

iii) *HD 92693*

The star HD 92693 lies in the Carina OB1 region. Very weak features due to the interstellar C_2 $R(0)$, $Q(2)$, $Q(4)$, and $Q(6)$ lines can be identified at $V_\odot = -13.5 \pm 1.5$ km s^{-1}. Their equivalent widths are consistent with those measured by Gredel and Münch (1986) at the same velocity after much longer exposure times. The total estimated C_2 column density is $(2.0 \pm 1.0) \times 10^{13}$ cm^{-2}. No reliable information about the physical conditions can be derived from the data. Interstellar C_2 was not detected toward the P Cygni–type variable star HD 94910 (AG Car), 3° away.

iv) *HD 94413*

The star HD 94413 lies in the direction of the Chamaeleon dark cloud and is labeled star "e" in the table and chart of Vrba and Rydgren (1984). Several interstellar C_2 lines can be identified in the CTIO data at a velocity $V_{LSR} = 4 \pm 3$ km s^{-1}, but the data are of too poor quality to constrain the physical conditions in the cloud. The implied total C_2 column density is substantial, $N(C_2) = (7 \pm 2) \times 10^{13}$ cm^{-2}.

A weak feature with $W_\lambda = 4.2 \pm 1.5$ mÅ has been found at the position of the $R_2(1)$ and $^RQ_{21}(1)$ blend in the CN (1, 0) red system band at the same velocity. The inferred CN column density in the $N'' = 1$, $J'' = 1/2 + 3/2$ levels is $(1.7 \pm 0.6) \times 10^{13}$ cm^{-2}, suggesting a total column density

$N(CN) \approx (5.7 \pm 2.0) \times 10^{13}$ cm^{-2} at $T_{ex} = 2.7$ K. Other important CN lines coincided with terrestrial H_2O features at the time of observations.

v) *HD 78344*

Various R and Q lines of interstellar C_2 with J'' up to 10 have also been seen in the spectrum of the star HD 78344 at $V_{LSR} \approx 9$ km s^{-1}. The C_2 excitation is consistent with $T \approx 40$ K and $n \approx 200$ cm^{-3}, and gives a total column density $N(C_2) \approx (8 \pm 3) \times 10^{13}$ cm^{-2}. No CN lines in the (1, 0) band were evident at this velocity at the level $W_\lambda \approx 3$ mÅ, suggesting a CN column density less than 10^{13} cm^{-2}.

vi) *HD 152236*

Weak features with $W_\lambda \approx 0.5$–1.0 mÅ belonging to the $R(0)$, $R(2)$, $Q(2)$, $Q(4)$, and $Q(6)$ lines of interstellar C_2 have been identified in the spectrum of HD 152236, but not in that of the nearby star HD 152235. The limited C_2 data suggest a relatively warm region, $T \geq 30$ K, with a low density, $n \approx 200$ cm^{-3}. The total C_2 column density for these conditions, $N(C_2) \approx (1.7 \pm 0.7) \times 10^{13}$ cm^{-2}, is comparable to that found in classical diffuse clouds. No CH or CN data have been obtained toward this star.

vii) *Other Stars*

Table 4 summarizes information on the lines of sight where no interstellar C_2 or CN lines were definitely detected. The illuminating star of the reflection nebula Cederblad 112, HD 97300, lies in the Chamaeleon dark cloud region (cf. Wesselius, Beintema, and Olnon 1984; Hyland, Jones, and Mitchell 1982). Also of interest is Elias 16 in the ρ Oph region. The star HDE 290861 lies in NGC 2071, a reflection nebula which is associated with a bipolar molecular outflow (Snell *et al.* 1984). Although suggestive features appear in the noise in the C_2 and CN spectra of this star, no convincing identification can be made for a sensible radial velocity. In these cases, the relatively poor signal-to-noise ratios of the spectra—rather than a true absence of molecules—may be responsible for the lack of detections. Failure to detect C_2, CN, or CH at lower levels would be surprising.

Marginal detections of interstellar C_2 have been made at CTIO toward the stars JM-1, Wray 977, HD 106391, and HD 113422. Only in the case of HD 106391 can a possible CN feature be identified at the same velocity as that of the possible C_2 lines.

IV. DISCUSSION

a) Correlation with Extinction

Table 9 summarizes the derived column densities for those lines of sight for which molecular lines have been detected. The table includes the results found for a number of well-studied diffuse clouds, such as the ζ Oph and ζ Per clouds, as well as the HD 29647 cloud observed by Crutcher (1985). References to the sources for the equivalent widths for lines of sight not studied in this work are given in van Dishoeck and Black (1986*a*) for the diffuse clouds, and in the footnotes for other clouds. All data have been reanalyzed in a consistent manner using the procedures described in § II. The results for some lines of sight in Cepheus and X Per are listed at the bottom of the table, but are generally not taken into account in the analysis because of the lower signal-to-noise ratio of these data, as well as the fact that most of the CH, C_2, and CN data were obtained by different observers using different instruments. For similar reasons, the data of Cardelli and Wallerstein (1986) for lines of sight in ρ Oph were not included. The adopted CN column density for HD 147889 is based on an equivalent width for the CN $R(0)$ feature of 26 ± 1 mÅ, as measured at the ESO CAT telescope with the CCD detector (C. P. de Vries 1987, private communication), together with a b-value of about 1.5 km s^{-1}. This new measurement falls midway between the value of 10.7 mÅ observed by Crutcher and Chu (1985) and the value of 36.7 mÅ obtained by Cardelli and Wallerstein (1986). The strength of the CH 4300 Å line toward HD 147889 has been remeasured at the ESO CAT telescope to be 38 ± 2 mÅ, in good agreement with $W_\lambda \approx 40$ mÅ found by Crutcher and Chu (1985), but again lower than $W_\lambda \approx 51$ mÅ found by Cardelli and Wallerstein.

TABLE 9

SUMMARY OF OBSERVED CH, C_2, AND CN COLUMN DENSITIES IN DIFFUSE AND TRANSLUCENT CLOUDS

Star	N(CH)	$N(C_2)$	N(CN)
HD 29647	$(1.5 \pm 0.5)(14)$[a]	$(1.7 \pm 0.3)(14)$[b]	$(1.6 \pm 0.3)(14)$[a]
HD 63804	...	$(1.7 \pm 0.6)(14)$	$(3.6 \pm 1.5)(13)$
HD 80077	$(1.1 \pm 0.3)(14)$	$(1.3 \pm 0.3)(14)$	$(4.0 \pm 0.6)(13)$
HD 94413	...	$(7.0 \pm 2.0)(13)$	$(5.7 \pm 2.0)(13)$
HD 110432	$(1.5 \pm 0.3)(13)$	$(3.0 \pm 1.0)(13)$	$(5 \pm 3)(12)$
o Sco	$(5.0 \pm 1.0)(13)$	$(5.5 \pm 1.0)(13)$	$(6 \pm 2)(12)$
HD 147889	$(1.0 \pm 0.3)(14)$[c,d]	$(1.2 \pm 0.3)(14)$[e]	$(1.4 \pm 0.4)(13)$[d]
HD 154368	$(8 \pm 2)(13)$	$(5.8 \pm 0.6)(13)$	$(3.5 \pm 0.5)(13)$
HD 169454	$(5.8 \pm 0.8)(13)$	$(7.0 \pm 1.4)(13)$	$(5.5 \pm 0.6)(13)$
ζ Per	$(2.0 \pm 0.3)(13)$	$(1.9 \pm 0.3)(13)$	$(3.0 \pm 0.3)(12)$
o Per	$(1.9 \pm 0.3)(13)$	$(2.2 \pm 0.3)(13)$	$(1.6 \pm 0.3)(12)$
ζ Oph	$(2.5 \pm 0.3)(13)$	$(2.4 \pm 0.3)(13)$	$(2.9 \pm 0.3)(12)$
χ Oph	$(3.4 \pm 0.3)(13)$	$(4.3 \pm 0.5)(13)$	$(1.3 \pm 0.3)(12)$
ρ Oph A	$(2.0 \pm 0.3)(13)$[f]	$(2.7 \pm 0.5)(13)$[g]	$(1.4 \pm 0.3)(12)$[h]
HD 206267	$(2.5 \pm 0.5)(13)$[i]	$(8.5 \pm 2.0)(13)$[j]	$(1.0 \pm 0.3)(13)$[i]
HD 207198	$(4.5 \pm 1.0)(13)$[i]	$(3.5 \pm 2.0)(13)$:[j]	$(5.0 \pm 2.0)(12)$[i,k]
λ Cep	$(1.8 \pm 0.5)(13)$[i]	2(13):[i]	$(2.0 \pm 0.5)(12)$[i]
X Per	$(3.0 \pm 0.5)(13)$[j]	5(13):[j]	$(8.5 \pm 2.0)(12)$[j]

[a] Crutcher 1985.
[b] Hobbs, Black, and van Dishoeck 1983.
[c] Crutcher and Chu 1985.
[d] de Vries 1987, private communication.
[e] van Dishoeck and de Zeeuw 1984.
[f] Danks, Federman, and Lambert 1984.
[g] Danks and Lambert 1983.
[h] Federman, Danks, and Lambert 1984.
[i] Chaffee and Dunham 1979.
[j] Federman and Lambert 1988.
[k] Crutcher, unpublished, as quoted by Joseph, Snow, and Seab 1988.

In Figures 8*a*–8*d*, the variations of the C_2, CH, and CN column densities with extinction are presented. In Figure 8*a* only those lines of sight for which C_2 has been detected are shown, whereas Figure 8*b* includes the upper limits on C_2 as open circles. Figures 8*a*–8*d* include the column densities for the classical diffuse clouds as well as the HD 29647 cloud. The open squares denote the column densities for stars in Cepheus.

Although there is a general increase in the C_2, CH, and CN column densities with $E(B-V)$ for lines of sight with detections, the scatter in the data is large for all three species. Figure 8*b* clearly illustrates that there is no close correlation between the C_2 column density and the extinction, as was proposed by Lutz and Crutcher (1983). The absence of such a correlation is not surprising, since many of the observed stars are distant supergiants, for which large fractions of the extinction are contributed by diffuse atomic clouds not associated with the molecular regions. This point is illustrated in Figure 8*c*, where

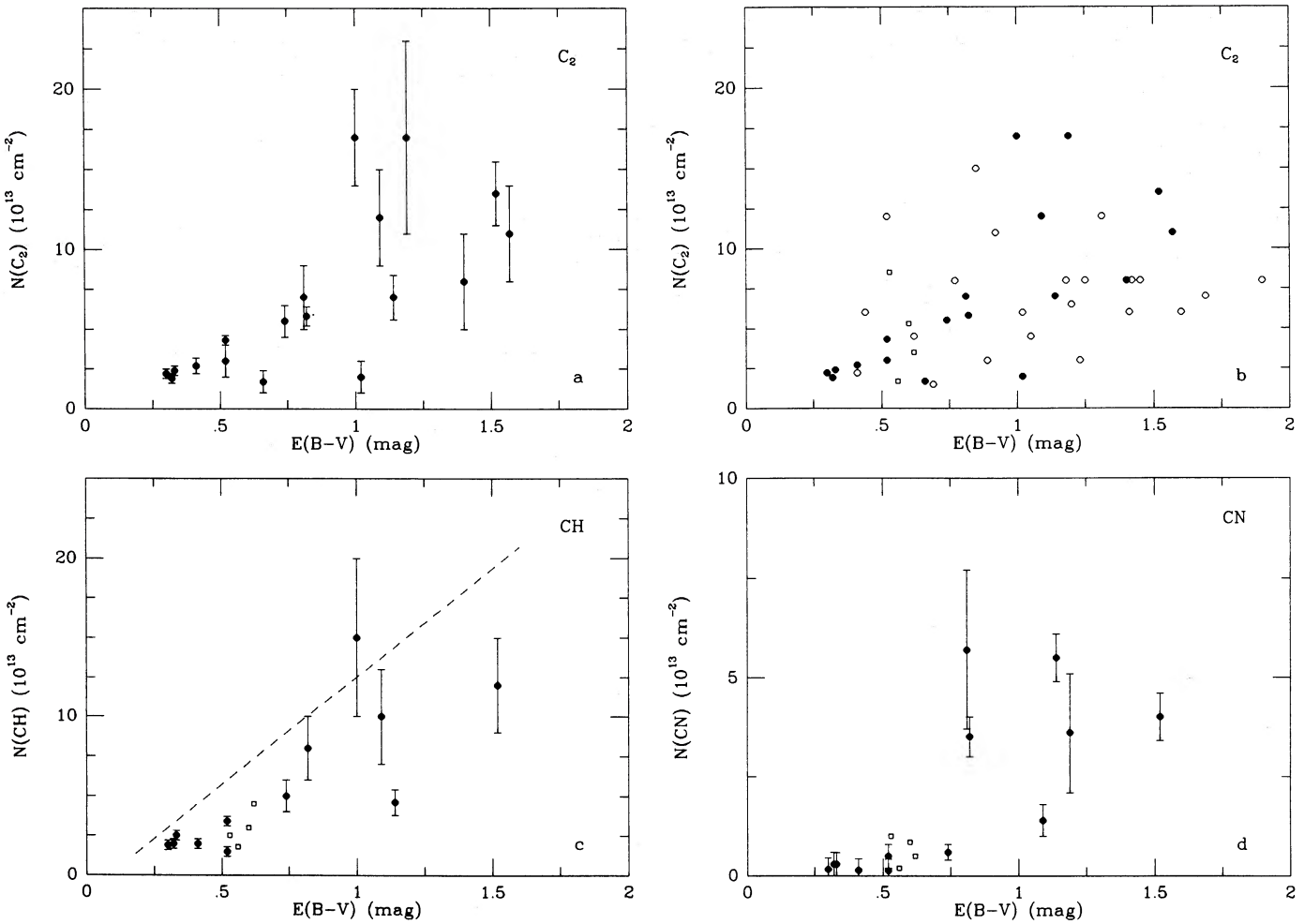

FIG. 8.—Molecular column densities as functions of extinction. (*a*) C_2 vs. $E(B-V)$ for lines of sight with detected C_2. (*b*) C_2 vs. $E(B-V)$ for all lines studied in this work. Filled circles denote lines of sight with detected C_2; open circles refer to upper limits. Open squares indicate the C_2 column densities measured by Federman and Lambert (1988) for lines of sight in Cepheus. (*c*) CH vs. $E(B-V)$ for lines of sight studied in this paper. The open squares indicate the column densities measured for stars in Cepheus by Chaffee and Dunham (1979) and Federman and Lambert (1988). The dashed line is the relation found by Mattila (1986) for dark clouds. The one point lying above this line refers to HD 29647. (*d*) CN vs. $E(B-V)$ for lines of sight studied in this work. Open squares indicate the CN column densities in the Cepheus region based on measurements by Chaffee and Dunham (1979), Joseph, Snow, and Seab (1988) and Federman and Lambert (1988).

the CH data are compared with the average relation found by Mattila (1986, 1988) for dark clouds from CH 9 cm observations. It appears that most of the data fall below the dashed line. Provided that the physical conditions such as density and carbon depletion are similar in these translucent clouds to those in the outer parts of the dark clouds studied by Mattila, this suggests that only part of the extinction is associated with molecular hydrogen in the clouds of our sample. In particular, HD 80077 and HD 169454 appear to have significant amounts of atomic gas in front of them. The only point which lies above the relation found by Mattila is for the nearby star HD 29647, which shines through a significant part of the Taurus molecular cloud. Note also that the extinction for this line of sight is unusual (Straižys, Wiśniewski, and Lebofsky 1982).

b) Correlation with H_2

It is clear that the extinction $E(B-V)$ provides only an upper limit to the H_2 column density along the line of sight, and that another indicator of the amount of molecular material needs to be found. The best candidate is probably provided by the CH molecule, for which a linear relation with H_2 has been established for diffuse clouds by Danks, Federman, and Lambert (1984). The work of Mattila (1986, 1988) suggests that the correlation also holds for larger extinctions in dark clouds. In addition, the CH chemistry is relatively well understood theoretically, since only a few reactions are involved in the formation of the molecule from H_2. In the following, we will therefore adopt the CH column density as a measure of the molecular hydrogen content of the cloud. A rough estimate of the actual H_2 column density can be obtained from the relation of Danks, Federman, and Lambert (1984),

$$\log N(H_2) = 1.125 \log N(CH) + 5.828 , \quad (3)$$

or that of Mattila (1986),

$$N(H_2) = 2.1 \times 10^7 N(CH) + 2.2 \times 10^{20} \text{ cm}^{-2} . \quad (4)$$

Note, however, that these are mean relations for a number of clouds, and that for individual clouds the CH/H_2 ratio may be different. For example, a higher than average radiation field, a lower gas-phase carbon abundance, and/or a lower density will lower the CH/H_2 ratio.

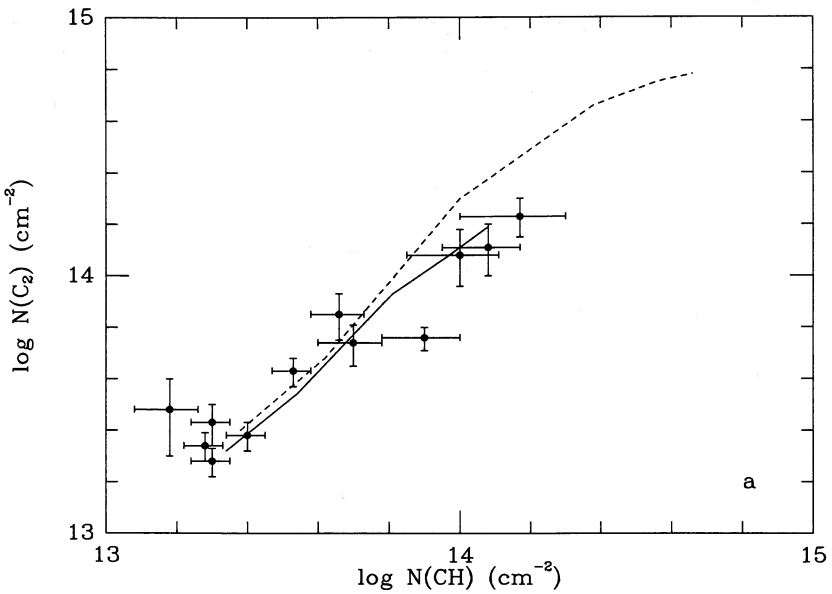

FIG. 9a

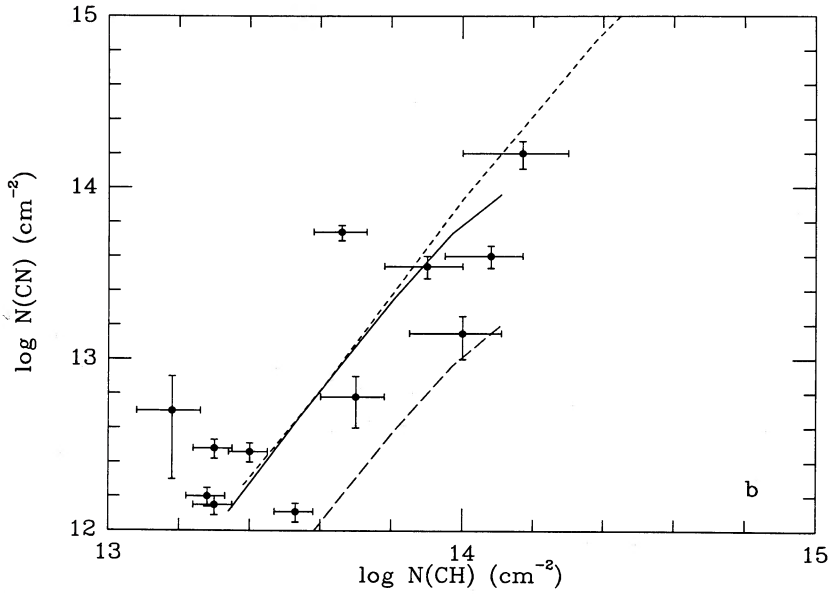

FIG. 9b

FIG. 9.—(*a*) Measured C_2 column densities as functions of measured CH column densities. The solid line indicates the theoretical relation found in models T1–T6 of Table 10 with $\delta_C = 0.1$, $\delta_O = 0.5$, $\delta_N = 0.6$ and $k_6 = 5 \times 10^{-16}$ cm^3 s^{-1}. The short-dashed line represents the model results for $\delta_O = 0.1$. (*b*) Same as (*a*) but for CN vs. CH. The long-dashed line shows the model results for $\delta_N = 0.1$.

In Figure 9*a* the measured C_2 column densities are plotted as functions of the measured CH column densities. A very good correlation between these two molecules is evident, and the scatter in this plot is much smaller than that in the relation of either species with $E(B-V)$. The relation can be represented well by the formula.

$$\log N(C_2) = 0.85 \log N(CH) + 2.2 , \qquad (5)$$

with a standard deviation of ± 0.15 in the fitted values of log $N(C_2)$. As will be discussed in more detail in § V, a close relation between the CH and C_2 column densities is not unexpected if C_2 is formed largely through the reaction of C^+ with CH.

In contrast with the close C_2–CH relation, the CN and CH data plotted in Figure 9*b* show a much larger scatter. There appear to be lines of sight such as the HD 29647 and HD 147889 clouds which have similar CH and C_2 column densities but for which the CN column densities differ by more than 1 order of magnitude. Other examples of large differences are provided by the *o* Sco and χ Oph clouds compared with the HD 169454 and HD 80077 clouds. If CN were formed mostly through the neutral-neutral reactions of C_2 and CH with N (Federman, Danks, and Lambert 1984), a much closer relation would have been expected. Possible explanations for these large variations will be discussed in § V.

The other major diatomic carbon-bearing molecule is CO. It

will be important to determine accurate CO column densities in more of the translucent regions where CH, C_2, and CN are observed.

V. COMPARISON WITH MODELS

Models of translucent clouds have been developed by van Dishoeck and Black (1988*a*), who studied in detail the photodissociation of CO in such clouds. This process, together with the ionization balance of carbon, controls the depth at which C^+, the dominant form of carbon at the edge of the cloud, is transformed into C and CO. Since the C^+ abundance is crucial for the formation of CH and C_2, it is important that its variation with depth into the cloud be well understood.

The gas-phase reactions important in the formation of CH, C_2, and CN were identified more than a decade ago (see, e.g., van Dishoeck and Black 1988*b* for a recent review). The formation of the carbon-bearing species is thought to be initiated by the radiative association reaction

$$C^+ + H_2 \rightarrow CH_2^+ + H\nu\,, \qquad (6)$$

for which the rate coefficient is still not well determined. Dissociative recombination of CH_2^+ with electrons produces CH. Alternatively, reactions of CH_2^+ with H_2 result in CH_3^+, which can then dissociatively recombine to form either CH or CH_2 with an uncertain branching ratio. Reactions of CH and CH_2 with C^+ lead to the formation of C_2. The processes responsible for the production of CN are more uncertain. The reaction

$$N + H_3^+ \rightarrow NH_2^+ + H\,, \qquad (7)$$

which was previously used to initiate the formation of the N-bearing molecules, is now thought to be negligibly slow at interstellar temperatures (Herbst, DeFrees, and McLean 1987). The only alternative routes to CN are then through neutral-neutral reactions between C_2 and CH with N (Solomon and Klemperer 1972; Federman, Danks, and Lambert 1984) or through reactions of hydrocarbon ions such as CH_2^+ and CH_3^+ with N. All neutral species are destroyed primarily by photodissociation at the edge of the cloud (see van Dishoeck 1988 for a review), while deeper inside, destruction through neutral-neutral reactions with O starts to compete.

The chemical network outlined above has been applied by van Dishoeck and Black (1986*a*, 1988*b*) to the classical diffuse clouds like the ζ Oph cloud. The primary aim of that work was to constrain the physical conditions in the clouds as closely as possible. Based on a variety of diagnostic techniques, the central densities in the clouds were found to be a few hundred cm^{-3}, and the central temperatures about 30–40 K. The strength of the radiation field was inferred to be enhanced by a factor I_{UV} of 3–5 over the average interstellar radiation field of Draine (1978) from the populations of the excited rotational levels of H_2. Given this physical structure of diffuse clouds, the observations of the CH molecule could be reproduced by adopting a rate coefficient $k_6 \approx (5\text{–}7) \times 10^{-16}$ cm^3 s^{-1} for reaction (6). This value is consistent with theoretical estimates (Herbst 1982), but close to the experimental upper limit of 1.5×10^{-15} cm^3 s^{-1} found by Luine and Dunn (1985) at $T = 15$ K. The C_2 observations could be reproduced only if the branching ratio for the dissociative recombination of CH_3^+ favors CH_2 rather than CH, so that a significant contribution to the C_2 formation comes from the reaction of C^+ with CH_2. However, if the CN photodissociation rate recommended by van Dishoeck (1988) is adopted and if reaction (7) is indeed slow, the models produce too little CN by nearly an order of magnitude.

The problems with the abundance of CN in diffuse clouds, and to a lesser extent that of C_2, could be alleviated if the strength of the radiation field is overestimated in the models. If the population of the H_2 $J = 5$ rotational level were caused partly by some other mechanism such as shocks, the scaling factor could be lowered to $I_{UV} = 1$–2. Such a reduction would be sufficient to remove most of the discrepancies. The inferred value of k_6 could in that case be lowered to $(2\text{–}3) \times 10^{-16}$ cm^3 s^{-1}. However, current magnetohydrodynamic (MHD) shock models (Draine 1986; Pineau des Forêts *et al.* 1986) cannot produce large populations in the H_2 $J = 6$ and 7 levels. The observed populations of these levels toward ζ Oph still require a significant enhancement of the radiation field. An alternative solution would be to lower the intensity of the radiation field not over the full wavelength region but only at $\lambda < 1000$ Å, where most of the CN and CO photodissociation occurs. Such modifications have been explored by van Dishoeck and Black (1988*a*), and can enhance the CN column densities by factors of a few. Note that the C_2 and CH abundances are not much affected by a change of the radiation field at $\lambda < 1000$ Å, since their photodissociation occurs mostly at 1000–1300 Å and 1500–3000 Å, respectively.

In summary, many of the problems in reproducing the observed abundances of molecules accurately in diffuse clouds may be attributed to uncertainties in that part of the radiation field at shortest wavelengths, which is responsible for destroying the molecules. The main difference between the modeling of the classical diffuse clouds and the translucent clouds studied in this work is the fact that no observations of excited H_2 are available for the more highly reddened lines of sight. Thus, no direct constraints exist on I_{UV}, which can be chosen arbitrarily to be of order unity. In the models presented here, we will continue to use the original radiation field of Draine (1978) as the reference without any modifications at $\lambda < 1000$ Å. We have, however, adopted slightly lower unattenuated photodissociation rates for CN and C_2 than are listed by van Dishoeck (1988) for $I_{UV} = 1$: 1.5×10^{-10} and 1.2×10^{-10} s^{-1}, respectively. Owing to the uncertainties in the photodissociation cross sections for these two species, and in the shape of the radiation field at the shortest wavelengths, this modification is well within the range of plausible values. For CH the cross sections are better known, and we have continued to employ the rate of van Dishoeck (1987) of 9.5×10^{-10} s^{-1}.

Consider first the CH and C_2 chemistries. Column densities of these species have been computed for the translucent cloud models T1–T6 of van Dishoeck and Black (1988*a*). These models have total visual extinctions A_V^{tot} ranging from 1 to 5 mag, densities n_H ranging between 500 and 1000 cm^{-3}, and temperatures between 15 and 40 K, with $I_{UV} = 1$. Such densities and temperatures are consistent with or slightly higher than those inferred from the C_2 rotational excitation. Initially, we have adopted $k_6 = 5 \times 10^{-16}$ cm^3 s^{-1} and a branching ratio η of CH_3^+ to CH_2 of 0.9 in the models, based on the diffuse cloud results. The CO photodissociation rate at each depth was calculated in a simplified manner according to the shielding functions given in Table 5 of van Dishoeck and Black (1988*a*). The resulting CO column densities differ slightly from those given in that paper. The results are also sensitive to the adopted gas-phase carbon abundance, which is specified by the depletion factor δ_C, where $\delta_C = 1$ implies an abundance of gas-

phase carbon in all forms of 4.67×10^{-4} relative to hydrogen. In the classical diffuse clouds, δ_C was constrained by the C and C^+ ultraviolet absorption lines to be $\delta_C \approx 0.3$–0.7. Unfortunately, no such observations are yet available for the more highly reddened lines of sight. If $\delta_C = 0.4$ is employed in the translucent cloud models, the resulting CH and C_2 column densities are too large by up to an order of magnitude compared with the observed values. There are several ways to obtain better agreement with observations. First, carbon may be more depleted onto grains in the translucent clouds compared with diffuse clouds. Table 10 and Figure 9 contain the results for the T1–T6 models with $\delta_C = 0.1$–0.15. It appears that they can reproduce the observations reasonably well. A smaller value of δ_C affects the C_2 abundance somewhat more than that of CH. Thus the slope of the C_2–CH relation is slightly lowered if carbon is more depleted. Similarly, a decrease in the density of the models would decrease the C_2 abundance by a larger factor than the CH abundance, since the abundance of C_2 depends approximately quadratically on density, whereas the CH abundance varies only linearly (Federman, Danks, and Lambert 1984).

Second, the incident radiation field may be enhanced for the translucent clouds, as was found for the diffuse clouds. Note that the data for lowest column density plotted in Figure 9 actually refer to the classical diffuse clouds for which $I_{UV} = 3$–5 has been deduced. The effect of an increase of I_{UV} is to shift the computed CH and C_2 column densities to smaller values along nearly the same line as found for $I_{UV} = 1$, i.e., the slope of the C_2–CH relation is preserved by increasing I_{UV}. For $I_{UV} = 3$–5, the observational data are consistent with a larger value of $\delta_C \approx 0.3$–0.4 for small A_V^{tot}. For larger $A_V^{tot} > 3$ mag, where photoprocesses play a smaller role, carbon still needs to be substantially depleted.

A third approach to the C_2–CH chemistry is to assume that the radiation field responsible for dissociating CH and C_2 has been overestimated in the diffuse clouds, and that a value $I_{UV} \approx 1$–2 is more appropriate. In that case k_6 can be lowered to $(1$–$2) \times 10^{-16}$ cm^3 s^{-1}, and the branching ratio η for CH_3^+ to form CH_2 may be lower than 0.9. A series of models with $k_6 = 2 \times 10^{-16}$ cm^3 s^{-1}, $\eta = 0.5$, and δ_C decreasing from 0.3 for the most diffuse clouds to 0.15 for the thicker clouds, is found to reproduce the observations equally well. Another reaction for which the rate coefficient is uncertain is

$$C^+ + CH \rightarrow C_2^+ + H\,, \qquad (8)$$

which leads to the formation of C_2. The rate coefficient may be higher at low temperatures than the value appropriate at $T \approx 300$ K, $k_8 = 7.6 \times 10^{-10}$ cm^3 s^{-1}, adopted in the models, since CH is a polar molecule (cf. Herbst and Leung 1986). However, variations of k_8 of a factor of 3 changed the resulting C_2 column densities by only a small amount.

The models reproduce quite well the empirical relations

TABLE 10

COMPUTED COLUMN DENSITIES[a] FOR TRANSLUCENT CLOUDS

Model[b]	δ_C	δ_O	δ_N	Gr.[c]	A_V^{tot}	H_2	CH	C_2	CN	CO	C^+	C	I(610 μm)[d]	I(370 μm)[d]
T1	0.15	0.5	0.6	2	0.7	5.0(20)	2.2(13)	2.1(13)	1.3(12)	2.5(14)	7.5(16)	1.6(15)	3.3(-8)	2.0(-7)
	0.15	0.1	0.6	2			2.4(13)	2.5(13)	1.8(12)	2.0(14)	7.5(16)	1.6(15)	3.2(-8)	2.0(-7)
	0.15	0.5	0.1	2			2.2(13)	2.1(13)	2.3(11)	2.5(14)	7.5(16)	1.6(15)	3.2(-8)	2.0(-7)
	0.15	0.5	0.6	2[e]			2.4(13)	3.0(13)	3.3(12)	5.2(14)	7.4(16)	2.5(15)	5.1(-8)	3.1(-7)
	0.15	0.5	0.6	2[f]			2.0(13)	1.8(13)	1.4(12)	2.7(14)	7.5(16)	1.5(15)	3.0(-8)	1.8(-7)
T2	0.1	0.5	0.6	2	1.3	1.0(21)	3.5(13)	3.5(13)	4.6(12)	2.1(15)	9.2(16)	3.7(15)	7.3(-8)	4.6(-7)
	0.1	0.1	0.6	2			4.2(13)	4.8(13)	7.4(12)	1.8(15)	9.3(16)	3.7(15)	7.2(-8)	4.5(-7)
	0.1	0.5	0.1	2			3.5(13)	3.5(13)	7.7(11)	2.1(15)	9.2(16)	3.7(15)	7.3(-8)	4.6(-7)
	0.1	0.5	0.6	2[e]			3.6(13)	4.3(13)	1.0(13)	1.2(16)	8.0(16)	5.5(15)	1.1(-7)	6.7(-7)
	0.1	0.5	0.6	2[f]			3.1(13)	2.8(13)	4.4(12)	3.0(15)	9.2(16)	3.1(15)	6.2(-8)	3.8(-7)
T3	0.1	0.5	0.6	2	2.0	1.5(21)	6.4(13)	8.5(13)	2.3(13)	1.9(16)	1.2(17)	1.6(16)	2.5(-7)	1.9(-6)
	0.1	0.1	0.6	2			1.0(14)	2.0(14)	8.5(13)	1.1(16)	1.2(17)	1.8(16)	2.7(-7)	2.0(-6)
	0.1	0.5	0.1	2			6.4(13)	8.7(13)	3.9(12)	1.9(16)	1.2(17)	1.6(16)	2.5(-7)	1.9(-6)
	0.1	0.5	0.6	2[e]			4.1(13)	4.6(13)	1.7(13)	6.0(16)	8.1(16)	9.9(15)	1.8(-7)	1.2(-6)
	0.1	0.5	0.6	2[f]			4.6(13)	5.3(13)	1.6(13)	3.1(16)	1.1(17)	1.0(16)	1.8(-7)	1.2(-6)
T4	0.1	0.5	0.6	2	3.0	2.2(21)	9.4(13)	1.2(14)	5.4(13)	7.5(16)	1.1(17)	3.3(16)	4.5(-7)	3.5(-6)
	0.1	0.1	0.6	2			2.5(14)	4.6(14)	7.3(14)	5.1(16)	1.2(17)	4.8(16)	5.2(-7)	4.6(-6)
	0.1	0.5	0.1	2			9.4(13)	1.2(14)	9.2(12)	7.5(16)	1.1(17)	3.3(16)	4.5(-7)	3.5(-6)
	0.1	0.5	0.6	2[e]			5.8(13)	5.4(13)	3.1(13)	1.2(17)	7.9(16)	1.7(16)	2.9(-7)	2.0(-6)
	0.1	0.5	0.6	2[f]			5.8(13)	7.4(13)	3.0(13)	9.8(16)	1.0(17)	1.6(16)	2.8(-7)	1.9(-6)
T5	0.1	0.5	0.6	2	3.9	3.0(21)	1.2(14)	1.5(14)	8.2(13)	1.4(17)	9.9(16)	4.8(16)	7.5(-7)	5.1(-6)
	0.1	0.1	0.6	2			3.6(14)	5.6(14)	1.7(15)	1.1(17)	1.0(17)	6.9(16)	9.3(-7)	6.7(-6)
	0.1	0.5	0.1	2			1.2(14)	1.6(14)	1.4(13)	1.4(17)	9.9(16)	4.7(16)	7.5(-7)	5.1(-6)
	0.1	0.5	0.6	2[e]			8.0(13)	7.9(13)	5.1(13)	1.9(17)	7.3(16)	2.3(16)	4.1(-7)	2.7(-6)
	0.1	0.5	0.6	2[f]			8.0(13)	1.1(14)	5.4(13)	1.7(17)	9.6(16)	2.6(16)	4.6(-7)	3.0(-6)
T6	0.1	0.5	0.6	2	5.2	4.0(21)	1.3(14)	1.3(14)	9.1(13)	2.5(17)	9.9(16)	4.4(16)	7.8(-7)	5.0(-6)
	0.1	0.1	0.6	2			4.6(14)	6.0(14)	3.0(15)	2.1(17)	1.1(17)	6.5(16)	1.1(-6)	6.9(-6)
	0.1	0.5	0.1	2			1.3(14)	1.3(14)	1.6(13)	2.5(17)	9.9(16)	4.4(16)	7.8(-7)	4.9(-6)
	0.1	0.5	0.6	2[e]			8.8(13)	6.5(13)	5.9(13)	2.9(17)	7.4(16)	2.3(16)	4.3(-7)	2.7(-6)
	0.1	0.5	0.6	2[f]			9.0(13)	9.2(13)	6.8(13)	2.6(17)	9.6(16)	2.6(16)	4.9(-7)	3.1(-6)

[a] In cm^{-2}.

[b] All models have $I_{UV} = 1$. See van Dishoeck and Black 1988*a* for more details of the models. The CO column densities were computed using the shielding functions of Table 5 of that paper.

[c] Adopted grain properties. Model 2 of Roberge, Dalgarno, and Flannery 1981 has been adopted throughout, unless indicated otherwise.

[d] Atomic carbon line intensities in ergs s^{-1} cm^{-2} sr^{-1}.

[e] The extinction curve of HD 204827 is used; all other optical properties are the same as in grain model 2.

[f] The extinction curve of HD 147889 is used; all other optical properties are the same as in grain model 2.

between CH column density and H_2 column density or A_V^{tot}. In particular, the model results of Table 10 for $\delta_C = 0.1$–0.15, $\delta_O = 0.5$, and $\delta_N = 0.6$ follow rather closely the relation of equation (4) (Mattila 1986) for $A_V^{tot} \leq 3$ mag and approach the relation of equation (3) (Danks, Federman, and Lambert 1984) at higher values of A_V^{tot}. In this sense, the CH chemistry can be said to be understood well enough to justify the use of CH as an indirect tracer of H_2 in translucent clouds. Note that, for a given value of δ_C, the CH and C_2 column densities do not continue to increase, but actually level off at large A_V^{tot}. This is because the formation rates for these species start to decrease significantly owing to the decrease in the C^+ abundance in the models, and their destruction starts to be dominated by reactions with atomic oxygen. If $\delta_C = 0.1$, the maximum CH column density of about 10^{14} cm^{-2} is obtained at $A_V^{tot} \approx 3$ mag and is close to the maximum CH column density that has been observed in any translucent cloud so far. Larger CH or C_2 column densities could arise in regions where carbon is less depleted.

It thus appears that the observed C_2–CH trend can be reproduced reasonably well by a variety of methods. Because the individual translucent clouds studied here may have quite different physical characteristics, it is not essential that the data be fitted by one homogeneous set of models with the same values for the parameters δ_C, n_H, and I_{UV}. For example, the inferred density from the C_2 excitation for the HD 80077 cloud is low, $n_H \approx 350$ cm^{-3}, whereas for the HD 147889 cloud, which has similar CH and C_2 column densities, it is much higher, $n_H \approx 1500$ cm^{-3}. In addition, the strength of the radiation field may vary from place to place. Studies of general trends need to be complemented with detailed analyses of individual clouds. Table 11 compares a few models with observations for specific lines of sight, such as the HD 29647 and HD 147889 clouds. The model for the HD 29647 cloud is equivalent to model T5, but with $\delta_C = 0.15$. The temperature and density structure in the HD 147889 model are based on the analysis of the C_2 rotational excitation by van Dishoeck and de Zeeuw (1984). The radiation field was taken to be enhanced

TABLE 11

COMPARISON BETWEEN MODEL AND OBSERVED COLUMN DENSITIES[a] FOR THE HD 29647 AND HD 147889 CLOUDS

Parameter/Species	Model[b]	NBV[c]	HD 29647[d]	Model[e]	HD 147889[f]
n_H (cm^{-3})	1000	800	...	1500	...
T (K)	15	10	...	50	...
I_{UV}	1	0.7	...	12	..
Grain[g]	2[g]	...	...	2[g]	...
δ_C	0.15	0.2	...	0.22	...
H_2	3.0(21)	2.9(21)	...	2.0(21)	...
H	2.2(20)	1.6(20)	2.3(19)[h]	8.3(20)	2(20)
H_3^+	3.8(14)	2.9(14)	...	1.5(14)	...
C	3.3(16)	4.0(16)	...	5.7(16)	...
C^+	1.1(17)	1.7(17)	...	4.1(17)	...
CO	2.9(17)	3.5(17)	(1–4)(17)	1.7(16)	8(17)
CH	1.1(14)	1.7(14)	(1.5 ± 0.5)(14)	7.3(13)	(1.2 ± 0.2)(14)
C_2	1.6(14)	1.6(14)	(1.7 ± 0.3)(14)	1.6(14)	(1.2 ± 0.3)(14)
C_2H	2.7(13)	1.1(13)	...	3.0(13)	...
CH_2	2.9(14)	1.1(13)	...	2.0(14)	..
C_3	2.8(13)	2.8(12)	...	2.2(13)	...
O	2.3(18)	1.7(18)	...	2.0(18)	...
OH	1.3(15)	7.2(15)	2(15):	4.8(13)	>2(14)
H_2O	2.0(15)	1.6(15)	...	2.6(13)	...
O_2	8.0(13)	1.9(15)	...	6.9(11)	...
HCO^+	3.4(12)	2.3(13)	3(13)	4.4(11)	...
H_2CO	4.0(10)	...	1(14)	7.8(8)	...
N	3.7(17)	3.4(17)	...	4.8(16)	...
NH	5.1(11)	1.6(15)	...	3.2(9)	...
CN	8.0(13)	2.5(14)	(1.6 ± 0.3)(14)	8.6(12)	(1.4 ± 0.4)(13)
HCN	2.4(12)	1.5(13)	3(13)	3.4(10)	...
C 610 μm[i]	5.6(−7)	...	...	1.0(−6)	...
C 370 μm[i]	3.7(−6)	...	...	6.1(−6)	...
A_V^{tot} (mag)	3.9	3.7	3.6	3.0	3.0

[a] In cm^{-2}.

[b] The model for the HD 29647 cloud is equivalent to model T5; $\delta_O = 0.5$ and $\delta_N = 0.6$ are adopted.

[c] Model 6 of Nercessian, Benayoun, and Viala 1988. The radiation field has been rescaled to that adopted here at $\lambda = 1000$ Å.

[d] Based on the observations of Crutcher 1985, Hobbs, Black, and van Dishoeck 1983, Wouterloot 1981, Wilson and Minn 1977, and Sume, Downes, and Wilson 1975.

[e] Model for the HD 147889 cloud. The temperature and density are constant with depth; $\delta_O = 0.5$ and $\delta_N = 0.1$ are adopted.

[f] Based on the observations of Crutcher and Chu 1985, van Dishoeck and de Zeeuw 1984, Wouterloot 1981, Encrenaz, Falgarone, and Lucas 1975, and Myers *et al.* 1978. The CO and OH lie largely behind the star.

[g] Adopted grain properties. In the HD 29647 model, the extinction curve of HD 204827 is used; in the HD 147889 model, the extinction curve of HD 147889 is used; all other optical properties are the same as in grain model 2 of Roberge, Dalgarno, and Flannery 1981.

[h] The column density inferred from large-beam measurements of self-absorption in the 21 cm line (Wilson and Minn 1977) assumes a spin temperature of 14 K.

[i] Intensity in ergs cm^{-2} s^{-1} sr^{-1}.

by a factor $I_{UV} \approx 10$ because of the presence of a large number of young stars in the immediate surroundings and because HD 147889 itself appears to be embedded in the cloud rather than behind it (Snow 1983*a*). The enhancement factor I_{UV} is not well determined, however, and models that fit the data equally well can be developed for $I_{UV} \approx 1$–20. A striking difference between the models of the lines of sight to HD 29647 and HD 147889 is the factor of 27 higher column density of OH in the former model. This difference is due primarily to the more intense ultraviolet radiation of the latter, which not only destroys OH more rapidly but also maintains a larger amount of C^+ (another destroyer of OH) throughout the cloud. The foreground OH column densities are potentially measurable through absorption lines in the near-ultraviolet and will provide an important test of the models. Models appropriate for the HD 169454 cloud have been presented by Jannuzi *et al.* (1988).

Detailed chemical models of the line of sight to HD 29647 in Taurus have also been published recently by Nercessian, Benayoun, and Viala (1988). Column densities from model 6 of Nercessian *et al.* are listed in Table 11 for comparison with our results. The parameters of the two models and the calculated column densities for many species are in good agreement, although the present model predicts significantly smaller amounts of O_2, HCO^+, NH, and HCN and rather larger column densities of CH_2 and C_3 than model 6 of Nercessian *et al.* The larger abundances of nitrogen-bearing molecules in the model of Nercessian *et al.* evidently result from their adoption of a high rate coefficient for the unusual reaction (7) of H_3^+ and N to form NH_2^+. The larger abundances of CH_2 and C_3 in our model are attributable to our use of a high value of the branching ratio, $\eta \approx 0.9$. Crutcher (1985) and Nercessian *et al.* have suggested that the adoption of severe depletion factors for electron donors like Si, S, Mg, and Fe keeps the fractional ionization low and thus helps maintain a high abundance of HCO^+ and—indirectly—of HCN. In our model, Mg and S are relatively undepleted, although most of the electrons still come from ionization of atomic carbon through most of the cloud. Moreover, the relatively high electron fraction $[n(e)/n(H_2) \approx 2 \times 10^{-5}]$ in the center of our model has a partly compensating effect on HCO^+ in that electron impact competes favorably with neutral collisions in exciting the lowest rotational transition. These effects will be discussed in more detail elsewhere.

The current CH and C_2 observations alone cannot distinguish between the various different interpretations. However, the abundances of a number of other species which are chemically related to CH and C_2 are affected differently in the various models and could potentially serve as diagnostics. In particular, the amount of atomic carbon is directly proportional to the depletion factor δ_C. Predicted C column densities and intensities for the C $J = 1 \rightarrow 0$ (610 μm) and $J = 2 \rightarrow 1$ (370 μm) fine-structure lines are included in Table 10 for the $\delta_C = 0.1$ models. For $\delta_C = 0.15$–0.3, the C line intensities are significantly higher. The abundance of the CH_2 molecule is greatly affected by the branching ratio of the CH_3^+ dissociative recombination, and is lowered by an order of magnitude if η is lowered from 0.9 to 0.1. Unfortunately, it is not yet possible to observe this molecule in the interstellar medium. Note that this branching ratio does not change the CH abundance, since most of the CH_2 photodissociates to CH. On the other hand, both the carbon abundance and the branching ratio affect the amount of C_2H in the models. Observations of C_2H at millimeter wavelengths may provide useful tests of the chemistry.

The CN observations cannot distinguish between the various approaches either. Table 10 includes the computed CN column densities in the various models, and Figure 9*b* compares the calculations with observations. Any approach which reproduces the C_2–CH relation gives CN column densities that are consistent with the average observed trend. The depletion factor of N has been taken to be $\delta_N \approx 0.6$ in all models, where $\delta_N = 1$ represents a gas-phase abundance of nitrogen in all forms of 1×10^{-4}. The effect on the CN–CH relation of an increase in I_{UV} is again to shift the calculated points along the same line to smaller column densities, since both CH and CN are destroyed by photodissociation. Similarly, a decrease in δ_C shifts the CN–CH points down along the same line. Finally, an increase in density in the model would enhance the CN abundance relative to that of CH, since the CN abundance varies at least quadratically with density (Federman, Danks, and Lambert 1984), and would thus increase the slope of the relation.

Although the models presented in Table 10 and Figure 9*b* can reproduce the average CN–CH relation fairly well, they cannot account for the large variations in the CN abundance found for some lines of sight. These variations cannot be caused simply by a larger scaling factor for the radiation field for lines of sight with anomalously low CN column densities, as was assumed by Federman and Lambert (1988), since this would also lower the CH and C_2 column densities accordingly. As mentioned in § IV, the CH and C_2 column densities for lines of sight with small CN abundances, such as HD 147889 and *o* Sco, are substantial and follow the "normal" C_2–CH relation found for other clouds. Although the CN abundance was found to be slightly more sensitive in our models to the scaling factor I_{UV} than the CH abundance, the relative difference in the decrease of their abundances with increasing I_{UV} was significantly less than a factor I_{UV}, and was found to depend on the total thickness of the cloud. The low CN abundance could be caused by a large specific depletion of N in some clouds; however, the nitrogen depletion factor would have to be lowered to as much as $\delta_N \approx 0.05$–0.1, while $\delta_N = 0.6$ in other clouds. Such specific variations in nitrogen depletion from cloud to cloud appear implausible. Variations in the density are also not a likely explanation if higher density is expected to yield a higher CN abundance: the HD 147889 cloud with a low CN abundance has been inferred to have a higher density than the HD 29647 cloud on the basis of the C_2 data. Another possible explanation might lie in an additional chemical source of CN in clouds with the highest CN abundance. For example, if NH_3 were formed on grain surfaces and released back into the gas phase, subsequent reactions with C^+ could enhance the CN production. However, the same grain reactions are also expected to produce CH_4 and H_2O, which would result in an enhanced production of CH as well. Thus, no specific enhancement of CN is expected to occur.

Alternatively, CN could be selectively more vulnerable to ultraviolet radiation in some clouds. Various studies (Seab, Snow, and Joseph 1981; Snow 1983*b*; Fitzpatrick and Massa 1988; Joseph, Snow, and Seab 1988) have drawn attention to the fact that the ultraviolet extinction curves for stars in the ρ Oph region are abnormally low. It is exactly for lines of sight in this region (HD 147889, *o* Sco, and χ Oph) that the CN abundance is very low.[5] On the other hand, lines of sight for which large CN abundances have been found, such as HD

[5] Note that an exception is provided by ρ Oph itself, for which the CN column density is similar to that found toward ζ Oph and ζ Per.

29647 and HD 169454, appear to have extinction curves which rise unusually steeply in the ultraviolet (Seab, Snow, and Joseph 1981; Cardelli and Savage 1988).

In order to examine the effects of the shape of the extinction curve on the results, we have incorporated into photorate calculations the measured extinction curves of HD 147889 and HD 204827, as parameterized by Fitzpatrick and Massa (1988). Compared with the average extinction curve of Seaton (1979), the HD 147889 curve has a higher 2200 Å bump but rises much more slowly at ultraviolet wavelengths. The extinction curve for HD 204827 is taken as an example of the opposite behavior, similar to the curves for HD 29647 and HD 169454, which are not available in convenient form: it has a weak 2200 Å bump, but its extinction at 1000 Å is a factor of 2 higher than that toward HD 147889. The extinction curve toward, for example, ζ Oph falls in between the HD 147889 and HD 204827 curves. The other grain properties, such as the albedo and the scattering phase function, have been taken to be similar to those of grain models 2 or 3 of Roberge, Dalgarno, and Flannery (1981).

Photodissociation rates have been computed for the different extinction curves at various depths into the model clouds. Table 12 summarizes the photorates of important species at the center of the ζ Oph model G and the T1–T6 models. It is apparent that the effects of the various extinction curves are largest for species such as CO and CN which photodissociate primarily at $\lambda < 1000$ Å, where the differences are largest. On the other hand, the variations for molecules like CH and C_2, which photodissociate primarily at longer wavelengths, are generally only a factor of 2. If photodissociation were the primary destruction mechanism of CN throughout these clouds, the effect of different extinction curves would be large enough to explain the observed large variations in CN column densities for relatively constant CH and C_2 column densities. Note that similarly large variations would be expected for CO in translucent clouds, where much of the gas-phase carbon is still in atomic form.

TABLE 12

CENTRAL PHOTORATES[a] IN TRANSLUCENT CLOUD MODELS

Model[b]	Grain[c]	CH	C_2	CN	CO[d]
T1.....	2	3.0(−10)	2.4(−11)	1.1(−11)	2.9(−11)
	2[e]	2.5(−10)	1.4(−11)	4.1(−12)	1.1(−11)
	2[f]	3.5(−10)	2.8(−11)	9.9(−12)	2.2(−11)
T2.....	2	2.5(−10)	1.7(−11)	4.7(−12)	2.6(−12)
	2[e]	2.0(−10)	8.7(−12)	1.2(−12)	3.2(−13)
	2[f]	2.9(−10)	2.2(−11)	4.3(−12)	1.3(−12)
T3.....	2	1.2(−10)	5.4(−12)	5.0(−13)	2.1(−13)
	2[e]	8.6(−11)	2.0(−12)	6.0(−14)	3.6(−15)
	2[f]	1.5(−10)	8.2(−12)	5.2(−13)	1.2(−13)
T4.....	2	5.8(−11)	1.8(−12)	6.2(−14)	9.2(−15)
	2[e]	4.0(−11)	4.6(−13)	2.9(−15)	5.4(−17)
	2[f]	8.2(−11)	3.4(−12)	6.7(−14)	2.3(−15)
T5.....	2	3.5(−11)	7.7(−13)	1.6(−14)	1.4(−15)
	2[e]	2.4(−11)	1.6(−13)	3.5(−16)	1.8(−18)
	2[f]	5.3(−11)	1.8(−12)	2.0(−14)	2.4(−16)
T6.....	2	1.1(−11)	1.2(−13)	1.1(−15)	1.4(−16)
	2[e]	8.1(−12)	1.9(−14)	1.4(−17)	2.0(−20)
	2[f]	2.0(−11)	4.8(−13)	2.5(−15)	8.6(−18)

[a] In s^{-1}.

[b] All rates are for $I_{UV} = 1$. See van Dishoeck and Black 1988*a* for further details of the models.

[c] Adopted grain properties. Model 2 of Roberge, Dalgarno, and Flannery 1981 is used unless indicated otherwise.

[d] Computed using the shielding functions given in Table 5 of van Dishoeck and Black 1988*a*.

[e] The extinction curve of HD 204827 is used; all other optical properties are the same as in grain model 2.

[f] The extinction curve of HD 147889 is used; all other optical properties are the same as in grain model 2.

The effects of different extinction curves are somewhat diminished, however, if depth-dependent calculations are performed. For example, in models T1–T4, the CN column densities differ by at most a factor of 3 for the various extinction curves, whereas the effect is even smaller for models T5 and T6. This insensitivity results from the fact that at a depth of only 1 mag into a cloud, the removal of CN by atomic oxygen,

$$\mathrm{CN} + \mathrm{O} \rightarrow \mathrm{CO} + \mathrm{N}\,, \qquad (9)$$

starts to compete with photodissociation if the rate for this reaction is as large as $k_9 = 1.0 \times 10^{-12} T^{1/2}$ cm^3 s^{-1}. As Table 12 shows, it is just at this depth that the differences in photorates for the various extinction curves start to become large. For CH and C_2, photodissociation continues to be important deeper into the cloud, but for these species the extinction curve has less influence. The effects are found to be somewhat larger for CO, because CO is not removed by reactions with neutrals, so that photodissociation remains important until deep into the cloud where removal by He^+ becomes substantial. Unfortunately, no reliable column densities of CO have yet been derived for these lines of sight. Although the rate of reaction (9) has been measured at room temperature with some component of vibrationally excited CN (Schmatjko and Wolfrum 1976), its behavior at low temperature for ground-state reactants is not known. If k_9 were lower by an order of magnitude, the CN column density would be more sensitive to variations in the extinction and radiation fields.

It is thus concluded that different shapes of the ultraviolet extinction curve cannot explain the large observed variations in CN abundances, even though they can cause order-of-magnitude differences in the central photorates. Variations in the gas-phase oxygen abundance from cloud to cloud may play a minor role: CN would be expected to be enhanced in clouds with large depletions of oxygen, because of its reduced removal rate through reaction (9). Although substantial ice mantling of the grains has been inferred for HD 29647 (Seab, Snow, and Joseph 1981), which is a cloud with a large CN abundance, the deduced amount of oxygen in the form of water on grains is comparatively small and is unlikely to cause order-of-magnitude variations. Nevertheless, an intriguing correlation has been found by Joseph, Snow, and Seab (1988) between the CN abundance and the grain properties: lines of sight with large CN abundances appear to have a relatively weak 2200 Å bump. No satisfactory explanation for this empirical result has yet been found.

In summary, the large observed variations from cloud to cloud in CN abundance, where C_2 and CH abundances are relatively constant, remain poorly understood quantitatively, although many different qualitative explanations can be identified. Perhaps a combination of several effects (e.g., selective O and N depletion together with abnormal extinctions) could be found which mimics the observations. Such specific depletions would also affect the abundances of other oxygen- or nitrogen-bearing species, however. Observational searches for molecules like OH and HCN could help to constrain the models further.

VI. CONCLUDING REMARKS

Through interstellar absorption-line observations of reddened stars, we have sought to identify a sample of translucent molecular clouds. The observations of CH, C_2, and CN provide useful information on the physical conditions in these clouds. The abundances of these simple species also constitute significant tests of theories of interstellar chemistry, in the physical regime in which the molecular content is high yet photoprocesses are still very important. The column densities of C_2 and CH are found to be strongly correlated with each other, and probably with the column density of H_2. Large variations in the CN abundance, however, pose a major problem for the understanding of the chemistry. The answer may lie in one or more of the following effects: (1) variable element depletions, (2) variations in the ultraviolet radiation field and extinction curve, and (3) uncertain rates for reactions that are essential for the nitrogen chemistry. Comparison of the observed abundances with theoretical cloud models elucidate some elements of the chemistry that are crucial and/or poorly understood. In the future, it will be important to observe additional atomic and molecular species in some of the translucent clouds identified here. In particular, there is a need for complementary measurements of radio emission lines. Further detailed investigations of individual clouds, similar to those carried out for the lines of sight to HD 29647 and HD 169454, would be valuable.

Technicians, telescope operators, and staff scientists of the European Southern Observatory, the Cerro Tololo Inter-American Observatory, and the Multiple Mirror Telescope Observatory provided invaluable assistance with the observational work reported here. The authors are indebted to C. P. de Vries for obtaining the CH and CN absorption-line data for HD 147889 and HD 80077. This work is supported in part by National Science Foundation grant RII 86-20342 to Princeton University, and in part by the National Aeronautics and Space Administration through Theoretical Astrophysics grant NAGW-763 to the University of Arizona. The hospitality of the Institute for Advanced Study is greatly appreciated.

REFERENCES

Balona, L., and Crampton, D. 1974, *M.N.R.A.S.*, **166**, 203.
Bauer, W., Becker, K. H., Bielefeld, M., and Meuser, R. 1986, *Chem. Phys. Letters*, **123**, 33.
Bauer, W., Becker, K. H., Hubrich, C., Meuser, R., and Wildt, J. 1985, *Ap. J.*, **296**, 758.
Bauschlicher, C. W., Jr., Langhoff, S. R., and Taylor, P. R. 1988, *Ap. J.*, **332**, 531.
Bernath, P. F. 1987, *J. Chem. Phys.*, **86**, 4838.
Black, J. H., and van Dishoeck, E. F. 1988, *Ap. J.*, **331**, 986.
Blades, J. C. 1978, *M.N.R.A.S.*, **185**, 451.
Blades, J. C., and Bennewith, P. D. 1973, *M.N.R.A.S.*, **161**, 213.
Bowers, P. F., Kerr, F. J., and Hawarden, T. G. 1980, *Ap. J.*, **241**, 183.
Brazier, C. R., and Brown, J. M. 1984, *Canadian J. Phys.*, **62**, 1563.
Brooks, J. W., Sinclair, M. W., and Manefield, G. A. 1976, *M.N.R.A.S.*, **175**, 117.
Brzozowski, J., Bunker, P., Elander, N., and Erman, P. 1976, *Ap. J.*, **207**, 414.
Cardelli, J. A., and Savage, B. D. 1988, *Ap. J.*, **325**, 864.
Cardelli, J. A., and Wallerstein, G. 1986, *Ap. J.*, **302**, 492.
Cartwright, D. C., and Hay, P. J. 1982, *Ap. J.*, **257**, 383.
Castor, J. I., and Simon, T. 1983, *Ap. J.*, **265**, 304.
Chabalowski, C. F., Peyerimhoff, S. D., and Buenker, R. J. 1983, *Chem. Phys.*, **81**, 57.
Chaffee, F. H., and Dunham, T. 1979, *Ap. J.*, **233**, 568.
Chaffee, F. H., and White, R. E. 1982, *Ap. J. Suppl.*, **50**, 169.
Chambaud, G., Lavendy, H., Levy, B., Robbe, J. M., and Roueff, E. 1988, *Chem. Phys.*, submitted.
Clemens, D. P., Sanders, D. B., Scoville, N. Z., and Solomon, P. M. 1986, *Ap. J. Suppl.*, **60**, 297.
Codina, S. J., de Freitas Pacheco, J. A., Lopez, D. F., and Gilra, D. 1984, *Astr. Ap. Suppl.*, **57**, 239.
Cohen, J. G. 1973, *Ap. J.*, **186**, 149.
Conti, P. S., Garmany, C. D., de Loore, C., and Vanbeveren, D. 1983, *Ap. J.*, **274**, 302.
Crutcher, R. M. 1985, *Ap. J.*, **288**, 604.
Crutcher, R. M., and Chu, Y.-H. 1985, *Ap. J.*, **290**, 251.
Crutcher, R. M., and Lutz, B. L. 1985, *Bull. AAS*, **16**, 937.
Danks, A. C., Federman, S. R., and Lambert, D. L. 1984, *Astr. Ap.*, **130**, 62.
Danks, A. C., and Lambert, D. L. 1983, *Astr. Ap.*, **124**, 188.
Davis, S. P., Shortenhaus, D., Stark, G., Engleman, R., Phillips, J. G., and Hubbard, R. P. 1986, *Ap. J.*, **303**, 892.
Davis, S. P., Smith, W. H., Brault, J. W., Pecyner, R., and Wagner, J. 1984, *Ap. J.*, **287**, 455.
de Vries, C. P., Brand, J., Israel, F. P., de Graauw, Th., Wouterloot, J. G. A., van de Stadt, H., and Habing, H. J. 1984, *Astr. Ap. Suppl.*, **56**, 333.
Dickman, R. L., Somerville, W. B., Whittet, D. C. B., McNally, D., and Blades, J. C. 1983, *Ap. J. Suppl.*, **53**, 55.
Douay, M., Nietmann, R., and Bernath, P. F. 1988, *J. Molec. Spectrosc.*, **131**, 250.
Draine, B. T. 1978, *Ap. J. Suppl.*, **36**, 595.
———. 1986, *Ap. J.*, **310**, 408.
Dufay, J., and Swings, P. 1958, *Ann. d'Ap.*, **21**, 260.
Enard, D. E. 1981, *The Messenger*, **26**, 22.
Encrenaz, P. J., Falgarone, E., and Lucas, R. 1975, *Astr. Ap.*, **44**, 73.
Engleman, R. 1974, *J. Molec. Spectrosc.*, **49**, 106.
Erman, P., Lambert, D. L., Larsson, M., and Mannfors, B. 1982, *Ap. J.*, **253**, 983.
Federman, S. R., Danks, A. C., and Lambert, D. L. 1984, *Ap. J.*, **287**, 219.
Federman, S. R., and Lambert, D. L. 1988, *Ap. J.*, **328**, 777.
Fitzpatrick, E. L., and Massa, D. 1988, *Ap. J.*, **328**, 734.
Garrison, R. F., Hiltner, W. A., and Schild, R. E. 1977, *Ap. J. Suppl.*, **35**, 111.
Gredel, R., and Münch, G. 1986, *Astr. Ap.*, **154**, 336.
Herbig, G. H., and Soderblom, D. R. 1982, *Ap. J.*, **252**, 610.
Herbst, E. 1982, *Ap. J.*, **252**, 810.
Herbst, E., DeFrees, D. J., and McLean, A. D. 1987, *Ap. J.*, **321**, 898.
Herbst, E., and Leung, C. M. 1986, *Ap. J.*, **310**, 378.
Hobbs, L. M., Black, J. H., and van Dishoeck, E. F. 1983, *Ap. J. (Letters)*, **271**, L95.
Huggins, P. J., Gillespie, A. R., Sollner, T. C. L. G., and Phillips, T. G. 1977, *Astr. Ap.*, **54**, 955.
Humphreys, R. M. 1978, *Ap. J. Suppl.*, **38**, 309.
Hyland, A. R., Jones, T. J., and Mitchell, R. M. 1982, *M.N.R.A.S.*, **201**, 1095.
Jannuzi, B. T., Black, J. H., Lada, C. J., and van Dishoeck, E. F. 1988, *Ap. J.*, **332**, 995.
Joseph, C. L., Snow, T. P., and Seab, C. G. 1988, *Ap. J.*, submitted.
Klare, G., and Neckel, Th. 1977, *Astr. Ap. Suppl.*, **27**, 215.
Klotz, R. 1987, private communication.
Knoechel, G., and Moffat, A. F. J. 1982, *Astr. Ap.*, **110**, 263.
Lada, E. A., and Blitz, L. 1988, *Ap. J. (Letters)*, **326**, L69.
Larsson, M., and Siegbahn, P. E. M. 1983, *J. Chem. Phys.*, **79**, 2270; **85**, 4208.
Larsson, M., Siegbahn, P. E. M., and Ågren, H. 1983, *Ap. J.*, **272**, 369.
Le Bourlot, J., Roueff, E., and Viala, Y. 1987, *Astr. Ap.*, **188**, 137.
Leitherer, C., and Wolf, B. 1984, *Astr. Ap.*, **132**, 151.
Luine, J. A., and Dunn, G. H. 1985, *Ap. J. (Letters)*, **299**, L67.
Lutz, B. L., and Crutcher, R. M. 1983, *Ap. J. (Letters)*, **271**, L101.
Mathis, J. S., Mezger, P. G., and Panagia, N. 1983, *Astr. Ap.*, **128**, 212.
Mattila, K. 1986, *Astr. Ap.*, **160**, 157.
———. 1988, *Astr. Ap.*, in press.
McKellar, A. 1954, *Pub. A.S.P.*, **66**, 312.
Meyer, D. M., and Hawkins, I. 1987, *Bull. AAS.*, **19**, 1054.
Middleburg, F. 1981, *IHAP Users Manual*, European Southern Observatory.
Miller, F. D. 1953, *Ap. J.*, **118**, 572.
Moffat, A. F. J., and FitzGerald, M. P. 1977, *Astr. Ap.*, **54**, 263.
Münch, G. 1964, *Ap. J.*, **140**, 107.
Myers, P. C., Ho, P. T. P., Schneps, M. H., Chin, G., Pankonin, V., and Winnberg, A. 1978, *Ap. J.*, **220**, 864.
Nercessian, E., Benayoun, J. J., and Viala, Y. P. 1988, *Astr. Ap.*, **195**, 245.
ONeil, S. V., Rosmus, P., and Werner, H.-J. 1987, *J. Chem. Phys.*, **87**, 2847.
Palmer, B. A., and Engelman, R. 1983, *Atlas of the Thorium Spectrum*, Los Alamos Nat. Lab. Rept. LA-9615.
Pineau des Forêts, G., Flower, D. R., Hartquist, T. W., and Dalgarno, A. 1986, *M.N.R.A.S.*, **220**, 801.
Pouilly, B., Robbe, J. M., Schamps, J., and Roueff, E. 1983, *J. Phys. B*, **16**, 437.
Riegel, K. W., and Crutcher, R. M. 1972, *Astr. Ap.*, **18**, 55.
Roberge, W. G., Dalgarno, A., and Flannery, B. P. 1981, *Ap. J.*, **243**, 817.
Rodgers, A. W. 1960, *M.N.R.A.S.*, **120**, 163.
Sanders, D. B., Clemens, D. P., Scoville, N. Z., and Solomon, P. M. 1986, *Ap. J. Suppl.*, **60**, 1.
Schild, R. E., Garrison, R. F., and Hiltner, W. A. 1983, *Ap. J. Suppl.*, **51**, 321.

Schmatjko, K. J., and Wolfrum, J. 1976, *Sixteenth Symposium (International) on Combustion* (Pittsburgh: Combustion Institute), p. 819.
Seab, C. G., Snow, T. P., and Joseph, C. L. 1981, *Ap. J.*, **246**, 788.
Seaton, M. J. 1979, *M.N.R.A.S.*, **187**, 73P.
Sneden, C., and Lambert, D. L. 1982, *Ap. J.*, **259**, 381.
Snell, R. L., Scoville, N. Z., Sanders, D. B., and Erickson, N. R. 1984, *Ap. J.*, **284**, 176.
Snow, T. P. 1983*a*, *Ap. J.*, **266**, 576.
———. 1983*b*, *Ap. J.* (*Letters*), **269**, L57.
Solomon, P. M., and Klemperer, W. 1972, *Ap. J.*, **178**, 389.
Souza, S. P., and Lutz, B. L. 1977, *Ap. J.* (*Letters*), **216**, L49.
Steemers, W. J. G., and van Genderen, A. M. 1986, *Astr. Ap.*, **154**, 308.
Straižys, V., Wiśniewski, W. Z., and Lebofsky, M. J. 1982, *Ap. Space Sci.*, **85**, 271.
Sume, A., Downes, D., and Wilson, T. L. 1975, *Astr. Ap.*, **39**, 435.
Taherian, M. R., and Slanger, T. G. 1984, *J. Chem. Phys.*, **81**, 3814.
Tapia, S. 1973, in *IAU Symposium 52, Interstellar Dust and Related Topics*, ed. J. M. Greenberg and H. C. van de Hulst (Dordrecht: Reidel), p. 43.
van Dishoeck, E. F. 1983, *Chem. Phys.*, **77**, 277.
———. 1984, Ph.D. thesis, University of Leiden.
———. 1987, *J. Chem. Phys.*, **86**, 196.
van Dishoeck, E. F. 1988, in *Rate Coefficients in Astrochemistry*, ed. T. J. Millar and D. A. Williams (Dordrecht: Kluwer), p. 49.
van Dishoeck, E. F., and Black, J. H. 1982, *Ap. J.*, **258**, 533.
———. 1984, *The Messenger*, **38**, 16.
———. 1985, *Bull. AAS*, **16**, 958.
———. 1986*a*, *Ap. J. Suppl.*, **62**, 109.
———. 1986*b*, in *Summer School on Interstellar Processes, Abstracts of Contributed Papers*, ed. D. J. Hollenbach and H. A. Thronson (NASA TM-88342), p. 149.
———. 1988*a*, *Ap. J.*, **334**, 771.
———. 1988*b*, in *Rate Coefficients in Astrochemistry*, ed. T. J. Millar and D. A. Williams (Dordrecht: Kluwer), p. 209.
van Dishoeck, E. F., and de Zeeuw, P. T. 1984, *M.N.R.A.S.*, **206**, 383.
Vrba, F. J., and Rydgren, A. E. 1984, *Ap. J.*, **283**, 123.
Walborn, N. R. 1972, *A.J.*, **77**, 312.
Wesselius, P. R., Beintema, D. A., and Olnon, F. M. 1984, *Ap. J.* (*Letters*), **278**, L37.
Whittet, D. C. B., and van Breda, I. G. 1980, *M.N.R.A.S.*, **192**, 467.
Wilson, T. L., and Minn, Y. K. 1977, *Astr. Ap.*, **54**, 933.
Wouterloot, J. G. A. 1981, Ph.D. thesis, University of Leiden.

Note added in proof.—While this work was in press, another *ab initio* theoretical study of the CN A–X system appeared (P. J. Knowles, H.-J. Werner, P. J. Hay, and D. C. Cartwright, *J. Chem. Phys.*, **89**, 7334 [1988]). Knowles *et al.* find a band oscillator strength $f_{20} = 9.0 \times 10^{-4}$, which is in good agreement with the theoretical result of Bauschlicher, Langhoff, and Taylor (1988), but still differs from the experimental determinations (see § II*d*).

JOHN H. BLACK: Steward Observatory, University of Arizona, Tucson, AZ 85721

EWINE F. VAN DISHOECK: Division of Geological and Planetary Sciences, California Institute of Technology 170-25, Pasadena, CA 91125